X chromosome and autosomal recombination are differentially sensitive to disruptions in SC maintenance

Katherine Kretovich Billmyre[1]*, Cori K. Cahoon[1,2]*, G. Matthew Heenan[1], Emily Wesley[1,5], Zulin Yu[1], Jay R. Unruh[1], Satomi Takeo[3], and R. Scott Hawley[1,4]

[1] Stowers Institute for Medical Research, Kansas City, MO, 64110, United States of America
[2]Institute of Molecular Biology, Department of Biology, University of Oregon, Eugene, United States of America
[3] Department of Biological Sciences, Tokyo Metropolitan University, Japan
[4] Department of Molecular and Integrative Physiology, University of Kansas Medical Center, Kansas City, KS, 66160, United States of America
[5] University of Missouri-Kansas City, Kansas City, MO, 64110, United States of America
* These authors contributed equally

Corresponding Author:
R. Scott Hawley
Stowers Institute for Medical Research
Kansas City, MO 64110
Phone (816) 926-4427
Fax (816) 926-2060
rsh@stowers.org

Key words: synaptonemal complex, meiosis, homologous recombination, crossing over

Abstract (150 words)

The synaptonemal complex (SC) is a conserved meiotic structure that regulates the repair of double strand breaks (DSBs) into crossovers or gene conversions. The removal of any central region SC component, such as the *Drosophila melanogaster* transverse filament protein C(3)G, causes a complete loss of SC structure and crossovers. To better understand the role of the SC in meiosis, we used CRISPR/Cas9 to construct three in-frame deletions within the predicted coiled-coil region of the C(3)G protein. These three deletion mutants disrupt SC maintenance at different times during pachytene and exhibit distinct defects in key meiotic processes, allowing us to define the stages of pachytene when the SC is necessary for homolog pairing and recombination. Our studies demonstrate that the *X* chromosome and the autosomes display substantially different defects in pairing and recombination when SC structure is disrupted, suggesting that the *X* chromosome is potentially regulated differently than the autosomes.

Introduction

Several facets of meiosis ensure the faithful inheritance of chromosomes from parents to offspring. During the creation of eggs and sperm the genome must be reduced to a haploid state containing a single set of chromosomes; the failure to properly segregate chromosomes results in chromosome missegregation, leading to gametes with an incorrect number of chromosomes. Indeed, errors in meiotic chromosome segregation are the leading cause of miscarriage and aneuploidy in humans, which can result in chromosomal disorders such as Down syndrome and Turner syndrome (reviewed in (Hassold et al., 2007)).

Proper segregation of chromosomes during meiosis relies on the formation of programmed double-strand breaks (DSBs), which are initiated when the evolutionarily conserved type II DNA topoisomerase-like protein, Spo11 (Mei-W68 in *Drosophila*), forms programmed DSBs (Keeney et al., 1997; McKim and Hayashi-Hagihara, 1998). These DSBs are then repaired as crossover or gene conversion events (Fig 1A,B). Crossovers mature into chiasmata, which physically hold homologous chromosomes together from nuclear envelope breakdown until homolog separation at anaphase I, thus ensuring proper segregation of chromosomes (Nicklas, 1974). The placement of crossover events is highly non-random and is strictly regulated by multiple processes (Hughes et al., 2018). First, crossover interference prevents two crossovers from occurring in close proximity to each other (Berchowitz and Copenhaver, 2010). Second, crossovers are excluded from the heterochromatin. Third, as a result of the centromere effect, crossing over is also reduced in those euchromatic regions that lie in proximity to the centromeres (Hughes et al., 2018). Finally, even within the medial and distal euchromatin, crossing over is substantially higher toward the middle of the chromosome arms (Szauter, 1984). These constraints do not affect the frequency or distribution of gene conversion events, which appear to be randomly distributed throughout the euchromatin (Crown et al., 2018; Miller et al., 2016, 2012). Thus, the control of crossover distribution may act at the level of DSB fate choice, rather than in determining the position of DSBs.

Previous studies have suggested that the synaptonemal complex (SC), a large protein structure that forms between homologous chromosomes, may play a role in controlling crossover distribution (Libuda et al., 2013). The SC is a highly conserved tripartite structure, with two lateral elements and a central region (Fig 1C) (reviewed in (Cahoon and

Hawley, 2016; Zickler and Kleckner, 2015, 1999)). The central region is composed of transverse filament and central element proteins, while the lateral element proteins connect the central region to the chromosome axes (Fig 1C). The known proteins that make up the *Drosophila* central region include the main transverse filament protein C(3)G, the transverse filament-like protein Corolla, and the central element protein Corona (CONA) (Collins et al., 2014; Page et al., 2008; Page and Hawley, 2001).

Work in *C. elegans* has shown that the SC functions to monitor crossover placement by preventing additional crossover designation in a region adjacent to an existing crossover precursor (Libuda et al., 2013; Nadarajan et al., 2017). Furthermore, there is evidence in *S. cerevisiae* that Zip1, a transverse filament protein, has two separable functions - one in building the SC and the other in recombination (Storlazzi et al., 1996; Voelkel-Meiman et al., 2016). Based on what is known in other model systems, it is likely that the *Drosophila* SC is also playing a role in regulating the fate of DSBs and monitoring crossover placement.

In *Drosophila*, approximately 24 DSBs are formed in early pachytene. This occurs in the context of fully formed SC after chromosome synapsis is already complete (Lake et al., 2013; Lindsley et al., 1977; Mehrotra and McKim, 2006). In the absence of the central region of the SC, DSB formation is substantially reduced, but not eliminated. Nonetheless, even in the presence of residual DSBs, there is a complete loss of crossover formation (Collins et al., 2014; Hughes et al., 2018; Mehrotra and McKim, 2006; Page et al., 2007). The abolishment of the central region of the SC also results in a high frequency of unpaired homologs during pachytene (Christophorou et al., 2013; Joyce et al., 2013; Sherizen et al., 2005; Takeo et al., 2011). In addition to disrupting

meiotic pairing, the loss of any of the known central region components in the (pre-meiotic) mitotic region of the ovaries also impairs mitotic pairing of the *2nd* and *3rd* chromosomes (Christophorou et al., 2013).

Since the vast majority of SC mutants are null mutants and therefore fail to form any SC structure, it is difficult to investigate the interactions of the wildtype versions of these proteins at the protein level or discover how the SC is involved in DSB repair and fate choice. In *Drosophila*, the study of transgenes carrying in-frame deletions of either the N- or C-terminal globular domains of C(3)G have shown that both of these regions are required for proper SC assembly and crossover formation (Jeffress et al., 2007). However, these defects were too severe to allow us to investigate the function of the SC in crossover placement and formation. One domain which has not been tested is the large predicted coiled-coil domain in C(3)G. Coiled-coil domains are a key conserved feature of transverse filament proteins across many organisms and are known to be important for protein-protein interactions (Lupas and Bassler, 2017).

Here we characterize three in-frame deletion mutations in the coiled coil domain of the *Drosophila melanogaster c(3)G*, all of which cause a partial loss of SC function at different stages in early meiosis. We take advantage of the different stages of SC loss to examine when the SC is necessary for multiple meiotic events such as pairing and recombination. Unlike any previously characterized *Drosophila* meiotic mutants (Baker and Hall, 1976; Hughes et al., 2018; Parry and Sandler, 1974), the effects of these mutants on *X* chromosome recombination is different from their effects on autosomal recombination. We infer from this observation that chromosomes can respond differently to a failure in SC maintenance. We also show that the SC in early pachytene is important for the

maintenance of euchromatic pairing, especially in the centromere-distal regions of the chromosome arms. The maintenance of *X* chromosome pairing is more sensitive to SC defects than is pairing maintenance on the autosomes, suggesting there may be additional chromosome-specific processes that mediate pairing. These mutants allow us for the first time to examine the temporal requirement for the synaptonemal complex in crossover placement and maintenance of pairing.

Results

A 213 amino acid in-frame deletion within the coiled-coil region of C(3)G impairs the maintenance of the SC in early-mid pachytene

The two previous studies of the functional anatomy of C(3)G have relied on the analysis of transgenic constructs bearing in-frame deletions (Jeffress et al., 2007; Page and Hawley, 2001). While extremely useful, transgenes have the disadvantage of non-endogenous expression levels and improper temporal expression. Based on previous studies in *S. cerevisiae* (Tung and Roeder, 1998) and in *Drosophila* (Page and Hawley, 2001), CRISPR/Cas9 was employed to construct an in-frame deletion, $c(3)G^{cc\Delta 1}$, removing the base pairs encoding 213 amino acids (L340-A552) from the 488 amino acid predicted coil-coiled domain of C(3)G (Fig 2A, See Methods).

We first asked if $c(3)G^{cc\Delta 1}$ mutants retained the ability to assemble and disassemble the SC with normal kinetics. In wild type flies, components of the central region of the SC are associated with paired centromeres during the pre-meiotic mitotic divisions (Christophorou et al., 2013; Joyce et al., 2013). By early pachytene these proteins are assembled as tripartite SC that is visible as long, continuous tracks of

Corolla and C(3)G (Fig 2B, Fig 2.1A). The SC remains fully assembled until mid-late pachytene (stages 5/7), at which point the SC is removed from the euchromatic chromosome arms but remains at the centromeres in mid pachytene (Fig 1B) (reviewed (Hughes et al., 2018)). We assessed SC assembly in homozygous *c(3)G*$^{cc\Delta 1}$ females using a Corolla antibody to mark the central region of the SC. In early pachytene the total length of the SC was similar to wildtype with a decrease in total SC length occurring in early-mid pachytene and a significant decrease in mid pachytene (Fig 2B,C; p=0.01). However, the SC which formed in early-mid pachytene showed obvious discontinuities (Fig 2B).

To determine whether or not the removal of a large region of the coiled-coil domain in *c(3)G*$^{cc\Delta 1}$ mutants changed the tripartite structure of the SC, we measured the distance between the C-termini of C(3)G. This was accomplished using a superresolution technique, Stimulated Emission Depletion (STED), in conjunction with a C(3)G C-terminal specific antibody (Anderson et al., 2005; Collins et al., 2014). In wild type controls the distance between the C-termini of C(3)G was 118.4 nm (±0.6 nm SEM), while the distance in *c(3)G*$^{cc\Delta 1}$ mutants was reduced to 67.8 nm (±0.1 nm SEM) (Fig 2.1C). The decrease in SC width is might be explained by the decreased length of C(3)G due to the 213 amino acids that were deleted. Because a single amino acid residue in a helix is predicted to be 0.15 nm in length, one would expect the decrease in length of a single C(3)G$^{cc\Delta 1}$ homodimer to be 32 nm. Therefore, the width of the SC (which contains C(3)G homodimers arranged in a head to head orientation) would be predicted to be reduced by 64 nm in *c(3)G*$^{cc\Delta 1}$ mutants. Although the observed 50 nm decrease in the width of the SC is less than expected, the difference may be due to

differences in the way that the C(3)G$^{cc\Delta 1}$ homodimer interacts with the oppositely oriented homodimer emanating from the other lateral element. Most importantly, the reduction in coiled-coil length created by removal of a large portion of the coiled-coil domain does not disrupt the formation of tripartite SC, as is illustrated by the two lateral tracks of C(3)G and the single track of Corolla observed using STED (Fig 2.1C,D).

Loss of SC maintenance in early-mid pachytene is correlated with a reduction in *X* chromosome crossing over

The progressive (or temporal) loss of SC in *c(3)G$^{cc\Delta 1}$* flies allowed us to determine whether or not the perdurance of full-length SC until early-mid pachytene was required for proper crossing over and/or crossover placement. We examined recombination on the *X* chromosome and found that the total amount of recombination along the entire chromosome was decreased from 63 cM to 11.8 cM (Fig 3A, Table 1). This reduction in exchange was clearly polar, a well-known attribute of recombination-deficient mutants in *Drosophila* (Baker and Hall, 1976). Specifically, the chromosomal region distal and medial to the centromere from *scute (sc)* to *vermillion (v)* exhibited a very low level of crossing over (3.7% of wild type) while the centromere-proximal region from *v* to *yellow$^+$ (y$^+$)* was only reduced to 31.3% of wild type (Fig 3A, Table 1).

The analysis of crossing over on the *3rd* chromosome did not reveal a reduction in total map length when comparing wild type and *c(3)G$^{cc\Delta 1}$* flies (Fig 3B, Table 2, 50.9 cM and 64.4 cM respectively). However, the pattern of exchange was again altered in a polar fashion, with a decrease in distal recombination between *roughoid (ru)* and *hairy*

196 *(h)* (Fig 3B, Table 2, 58.2% of wild type) and a large increase (to 447% of wild type) in
197 the centromere-proximal region between *scarlet (st)* and *curled (cu)* (Fig 3B, Table 2).
198 To ensure the *3rd* chromosome recombination phenotype was representative of
199 both large autosomes, we examined recombination on the *2nd* chromosome. As shown
200 in Fig 3.1 and Table 3, the effect of the $c(3)G^{cc\Delta 1}$ deletion on *2nd* chromosome
201 recombination mirrored that observed for the *3rd* chromosome with a decrease in distal
202 recombination and a large increase on centromere-proximal exchange (Fig 3.1, Table
203 3). The greater than 300% increase in recombination across the centromere-proximal
204 region on both the *2nd* and *3rd* chromosomes suggests that normal, full-length SC in
205 early-mid and mid pachytene is regulating, directly or indirectly, crossover placement
206 along the length of the chromosome.
207 The striking difference in recombination patterns between the *X* chromosome
208 and autosomes suggest that the *X* chromosome responds differently to aberrations in
209 the SC in early-mid pachytene than the autosomes. Such chromosome-specific defects
210 in recombination have not been previously documented in *Drosophila* (Hughes et al.,
211 2018; Parry and Sandler, 1974).
212
213 **Smaller in-frame deletions within the putative coiled-coil domain also cause a**
214 **loss of SC maintenance**
215 One potentially confounding factor in the analysis of the $c(3)G^{cc\Delta 1}$ mutants was the
216 decrease in the width of the SC (Fig 2.1C) caused by the removal of a large region of
217 the coiled-coil domain. The deletion of such a large region of the coiled coil could
218 change the ability of the C(3)G protein to interact with itself and form stable SC but it

might also remove sites important for interacting with other proteins. Therefore, in an attempt to separate the multiple phenotypes seen in *c(3)G*^{ccΔ1} flies, we created two smaller deletions within the larger deletion, *c(3)G*^{ccΔ2} (D346-T361) and *c(3)G*^{ccΔ3} (K465-V471) (Fig 4A). These smaller regions should not significantly affect the length of the C(3)G protein based on the small number of amino acids deleted. These sites were picked based on regions of C(3)G where the COILS score (Lupas et al., 1991) dipped suggesting a loss of coiled-coil structure (Fig 4.1A). We hypothesized these might be regions important for regulation of SC structure and/or function, independent of SC width.

When SC formation in *c(3)G*^{ccΔ2} and *c(3)G*^{ccΔ3} mutants were examined by Corolla staining, *c(3)G*^{ccΔ2} flies displayed a similar SC length to wild type in early and early-mid pachytene, but displayed a decrease in total SC length in mid pachytene when compared to wild type (Fig 4B,C, $p=0.002$). However, *c(3)G*^{ccΔ3} mutants never formed fully assembled full-length SC (Fig 4B,C, $p<0.0001$). Although each of these deletions is much smaller than the *c(3)G*^{ccΔ1} deletion, *c(3)G*^{ccΔ2} mutants did not display a loss of SC length until mid pachytene, while *c(3)G*^{ccΔ3} mutants had a more severe loss of SC in early pachytene compared to *c(3)G*^{ccΔ1} mutants (Fig 2B and 4B). We confirmed through antibody staining that the SC that did assemble in *c(3)G*^{ccΔ2} and *c(3)G*^{ccΔ3} mutants contained C(3)G (Fig 4.1B,C) in addition to Corolla (Fig 4B). The drastic differences in SC formation and maintenance observed in these mutants gave us a tool to examine the requirement of SC in early pachytene vs mid pachytene without the removal of a large structural region of C(3)G.

242 **Full-length SC in mid pachytene is not necessary for *X* recombination**

243 When compared to *c(3)G*^{ccΔ1} flies, the *c(3)G*^{ccΔ2} mutants exhibited very different
244 recombination phenotypes. First, *c(3)G*^{ccΔ2} mutants had relatively normal levels of
245 recombination along the *X* chromosome (109% of wild type, Table 1, Fig 5A) but still
246 displayed increased centromere-proximal recombination on the *3rd* chromosome in the
247 *st-cu* interval (347% of wild type, Table 2,Fig 5C). Centromere-distal recombination
248 between *ru-h* on the *3rd* chromosome was reduced to 65.5% of wild type levels in
249 *c(3)G*^{ccΔ2} (Fig 5C, Table 2).

250 In contrast to *c(3)G*^{ccΔ2}, the *c(3)G*^{ccΔ3} deletion greatly reduced recombination on
251 the *X* chromosome to 4.5% of wild type (Fig 5B, Table 1). This reduction was similar to,
252 but more severe than, the reduction in *X* recombination seen in *c(3)G*^{ccΔ1} mutants
253 (18.7% of wild type, Table 1, Fig 3A). Additionally, *c(3)G*^{ccΔ3} mutants mimicked the *3rd*
254 chromosome recombination pattern we saw in *c(3)G*^{ccΔ1} and *c(3)G*^{ccΔ2} (Fig 3B, Fig 5C,
255 Table 2) with a centromere-distal reduction and a large centromere-proximal increase in
256 recombination (Fig 5D, distal = 25.5% of wild type, proximal = 404% of wild type). These
257 large increases in proximal exchange parallel those observed in *c(3)G*^{ccΔ1} mutants for
258 both the *2nd* and *3rd* chromosomes. We note that in all cases the mutant and control
259 crosses carry identical pericentromeric regions and therefore the observed effects on
260 exchange in the centromere-proximal regions of the autosomes cannot be attributed to
261 unrelated structural changes (See Methods).

262

263 **DSB formation in *c(3)G*^{ccΔ1}, *c(3)G*^{ccΔ2}, and *c(3)G*^{ccΔ3} mutants**

To confirm that the decreases in *X* chromosome recombination observed in both the *c(3)G*^{ccΔ1} and *c(3)G*^{ccΔ3} mutants were not due to a large decrease in the formation of DSBs, we assessed DSB formation using γH2AV, a phosphorylated form of the histone variant H2AV that specifically marks sites of DSBs. Although both *c(3)G*^{ccΔ1} and *c(3)G*^{ccΔ3} flies exhibited normal kinetics for DSB repair from early to mid pachytene, *c(3)G*^{ccΔ1} flies (but not *c(3)G*^{ccΔ3} flies) displayed a decrease in the number of DSBs formed in early pachytene (Fig 5.1A, p=0.03). Because *X* chromosome recombination was more severely affected in *c(3)G*^{ccΔ3} flies compared to *c(3)G*^{ccΔ1} flies, we do not believe the early pachytene decrease in *c(3)G*^{ccΔ1} mutants is biologically relevant to the decrease in crossing over on the *X* chromosome. Lastly, we assessed DSB formation in *c(3)G*^{ccΔ2} flies and saw a slight decrease in the number of DSBs formed in early pachytene compared to wild type (Fig 5.1A, p=0.006). However, since *c(3)G*^{ccΔ2} flies did not have an overall decrease in the formation of crossovers, the decrease in γH2AV may not be biologically significant.

One possible explanation for the increase in centromere-proximal recombination might be the induction of ectopic DSBs within the heterochromatin that were not induced by Spo11. To confirm that the centromere-proximal recombination was due to Spo11 breaks, we constructed a double mutant with *c(3)G*^{ccΔ3} and *vilya*^{826}, a recombination nodule component that is necessary for the induction of Spo11-induced breaks (Lake et al., 2015). When we assessed *3rd* chromosome recombination we saw very low levels of recombination (total map length = 1.4 cM, Fig 5.1B), similar to the recombination seen in *vilya*^{826} alone (Lake et al., 2015). This confirmed that the

286 crossovers in *c(3)G*$^{cc\Delta 3}$ mutants are due to programmed Spo11 DSBs and not an
287 increase in DNA damage.
288
289 **Chromosome segregation in *c(3)G*$^{cc\Delta 1}$, *c(3)G*$^{cc\Delta 2}$, and *c(3)G*$^{cc\Delta 3}$ mutants**
290 All previously characterized mutants in *Drosophila* that are unable to form crossovers,
291 or have a significant reduction in crossovers genome-wide, display high levels of both *X*
292 and *4th* chromosome nondisjunction (Collins et al., 2014; Krishnan et al., 2014;
293 Manheim and McKim, 2003; Page and Hawley, 2001; Yan and McKee, 2013). The high
294 levels of *X* nondisjunction observed in these recombination-defective mutants involves
295 the interactions between both non-crossover *X* chromosomes and non-crossover
296 autosomes (Baker and Hall, 1976; Hughes et al., 2018), such that two *X* chromosomes
297 segregate from one autosome with the remaining autosomes segregating at random. In
298 the absence of non-crossover autosomes, non-crossover *X* chromosomes will
299 segregate normally.
300 When the rate of missegregation of the *X* and *4th* chromosomes was assessed in
301 all three mutants, neither *c(3)G*$^{cc\Delta 1}$ or *c(3)G*$^{cc\Delta 2}$ mutants showed significantly increased
302 levels of *X* or *4th* chromosome nondisjunction when compared to wild type (Table 4).
303 *c(3)G*$^{cc\Delta 3}$ mutants displayed low levels of *X* (4.5%) and *4th* (2.0%) non-disjunction (Table
304 4). However, this low level of non-disjunction is much lower than the 39.2% reported in
305 *c(3)G* null mutants where the SC is completely absent (Hall, 1972).
306 The absence of an observed increase in *X* nondisjunction in *c(3)G*$^{cc\Delta 1}$ and
307 *c(3)G*$^{cc\Delta 2}$ mutants is most likely explained by the absence of the nonexchange
308 autosomes required to induce *X* chromosome nondisjunction. However, the low levels

of *X* nondisjunction observed in *c(3)G*$^{cc\Delta 3}$ mutants might also be compatible with a proposed role for C(3)G-like proteins in mediating achiasmate segregations (Gladstone et al., 2009; Previato de Almeida et al., 2019). Therefore, the severe SC fragmentation present in *c(3)G*$^{cc\Delta 3}$ mutants may cause a mild segregation defect even in the presence of autosomal recombination.

The loss of full-length SC in these mutants parallels the decrease in euchromatic homolog pairing

Homolog pairing is reduced in mutants lacking SC (Gong et al., 2005; Page et al., 2008; Sherizen et al., 2005). Thus, since our mutants exhibit SC defects in early to mid pachytene, we utilized them to investigate the importance of full-length SC in the maintenance of homolog pairing in *Drosophila*. Fluorescence In Situ Hybridization (FISH) was used to examine homologous pairing, and to mark the distal and proximal loci of the *X* chromosome.

In wild type, 90% to 100% of the *X* chromosome was paired from early to mid pachytene (Fig 6A). To determine what the baseline level of pairing is in the absence of the SC, *X* chromosome pairing was assessed in females homozygous for a null allele of *c(3)G* (*c(3)G*^{68}). In this genotype the centromere-distal region of the chromosome was most affected, with an average of 37% paired between early and early-mid pachytene, while the centromere-proximal region was paired in about half the nuclei (Fig 6.1A, 51.5%).

Starting at early-mid pachytene *c(3)G*$^{cc\Delta 2}$ mutants exhibited a slight pairing defect at the centromere-distal locus of the *X* chromosome (Fig 6A, early= 90.9%, early-mid

pachytene= 75%, mid pachytene= 58.8%) but were relatively well-paired at the centromere-proximal locus (Fig 6A, early=93.9%, early-mid pachytene= 95%, mid pachytene= 88.2%). Both *c(3)G*^{ccΔ1} and *c(3)G*^{ccΔ3} mutants displayed a progressive loss of pairing at both proximal and distal loci on the *X* chromosome. *c(3)G*^{ccΔ1} mutants had almost a complete loss of distal pairing by mid pachytene while *c(3)G*^{ccΔ3} mutants only maintained 26% pairing (Fig 6A).

These abnormalities in pairing maintenance correspond well with the recombination pattern seen on the *X* chromosome in *c(3)G*^{ccΔ1} and *c(3)G*^{ccΔ3} mutants in the sense that the distal region of the *X* chromosome was more affected than the proximal regions (Fig 3A and 6A). The centromere-distal decrease in recombination on the *3rd* chromosome in *c(3)G*^{ccΔ1} and *c(3)G*^{ccΔ3} mutants is displayed in conjunction with a similar loss of pairing. We examined pairing at distal, medial, and proximal loci on the *3rd* chromosome throughout pachytene. Similar to the *X* chromosome, both *c(3)G*^{ccΔ1} and *c(3)G*^{ccΔ3} mutants displayed a similar trend of reduced pairing of the *3rd* chromosome, with a progressive decrease in centromere-distal pairing that mirrors the recombination data (Fig 6B). The medial and proximal region of the *3rd* chromosome remained relatively paired from early to mid pachytene (Fig 6B). It should be noted that in *c(3)G*^{68} null mutants pairing on the *3rd* chromosome was more strongly reduced; however, the proximal region (45% paired) was still paired more frequently than was the distal region (35% paired) (Fig 6.1A).

To confirm that the loss of distal pairing on the *3rd* chromosome observed in *c(3)G*^{ccΔ1} and *c(3)G*^{ccΔ3} mutants was representative of the autosomes, we also examined pairing on the *2nd* chromosome in *c(3)G*^{ccΔ1} mutants. Pairing on the *2nd*

chromosome mirrored that of the *3rd* chromosome with a progressive loss of distal pairing but very little effect on medial and proximal pairing (Fig 6.1B). The significant loss of distal pairing might explain why there are stronger recombination defects in the distal regions of both the *X* and *3rd* chromosomes in $c(3)G^{cc\Delta 1}$ and $c(3)G^{cc\Delta 3}$ flies. By the same reason, the autosomal pairing that is maintained in these mutants is proximal, which may allow for an increased number of recombination events that are proximal to the centromere.

Centromere pairing in meiosis is not affected in the absence of full-length SC

In wild type *Drosophila* females, the eight centromeres (two for each of the four chromosomes) pair in the pre-meiotic cysts and then cluster into an average of two clusters by early pachytene (Takeo et al., 2011). The SC is important for centromere clustering in early meiotic cells with an average of four clusters in *c(3)G, cona* and *corolla* null mutants (Collins et al., 2014; Takeo et al., 2011; Tanneti et al., 2011). Using an antibody against CID, a centromere specific histone, we assessed if centromere clustering was altered in the context of SC loss in early to mid pachytene.

Oocytes from both wild type, $c(3)G^{cc\Delta 1}$, and $c(3)G^{cc\Delta 2}$ flies contained an average number of clusters from 1.7 to 2.5 foci in early to mid pachytene (Fig 6.2A,B). $c(3)G^{cc\Delta 1}$ mutants did display significantly more clusters than controls in early and mid pachytene (Fig 6.2A, p= 0.01 and 0.002 respectively). However, because the average was 2.5 foci, the loss of SC is not likely to be impacting centromere pairing in $c(3)G^{cc\Delta 1}$. $c(3)G^{cc\Delta 3}$ mutants had an average of 3.6 clusters in all three stages (Fig 6.2B, p< 0.001),

377 suggesting that SC assembly defects in early pachytene may be sufficient to disrupt
378 centromere clustering but not centromere pairing.
379

380 ## Discussion

381 The SC plays multiple roles during meiosis that illustrate its importance in ensuring the
382 successful transmission of genetic information from one generation to the next, yet our
383 knowledge of how the SC is involved in regulating meiotic processes, such as
384 recombination and the maintenance of pairing, is limited due to the integral nature of
385 each SC component. Here we report the first partial loss-of-function SC mutations in a
386 central region component in *Drosophila*. We use the different stages of SC loss found in
387 these mutants to show there is a temporal requirement of the SC in the regulation of
388 crossover number and placement on the *X* chromosome versus the autosomes (Fig 7).
389 Additionally, full-length SC is important for maintaining euchromatic homolog pairing in
390 distal chromosomal regions.
391

392 **Regulation of SC assembly and disassembly**

393 Both the regulation of SC assembly and disassembly, and it's maintenance after
394 assembly, is poorly understood. Work in other organisms has shown that post-
395 translational modifications are important in SC structure and function. It is known that
396 SUMOylation promotes assembly of the SC while phosphorylation promotes
397 disassembly of the SC with modifications occurring on multiple SC proteins (Jordan et
398 al., 2012; Nadarajan et al., 2017; Sato-Carlton et al., 2017). Thus far, no post-
399 translationally modified sites have been identified on C(3)G. However, it is likely that

these sites do exist, and we speculate that sites promoting SC assembly, maintenance, and disassembly may be disrupted in these mutants.

Another possibility is that the deletions described here could destabilize protein-protein interaction sites between C(3)G and other central region proteins resulting in unstable SC that is difficult to maintain. We note that the mutant with the smallest deletion, *c(3)G*^{ccΔ3}, exhibited the strongest SC defect. While this deletion was predicted to only disrupt a single coil, the best explanation for the more severe phenotype is that it actually disrupts the coiled-coil. This may have caused a large disruption in the rest of the coiled-coil structure. In the future, it will be important to further dissect these domains to better understand the regulation of SC assembly and disassembly.

A role for the SC in the maintenance of homolog pairing

A surprising result from these studies was the ability of these deletions to allow the progressive loss of homologous euchromatic pairing through pachytene. The mechanism behind establishing and maintaining homolog pairing is a long-standing, unanswered question in the meiosis field. Previous work in *Drosophila* has shown that in the complete absence of the central region proteins C(3)G and CONA, euchromatic pairing is significantly reduced in early-mid and mid pachytene (Gong et al., 2005; Page et al., 2008; Sherizen et al., 2005).

Our partial loss-of-function mutations have allowed us to test the importance of C(3)G in maintaining pairing throughout pachytene when SC is present in early pachytene (unlike previous studies of null mutants in which the SC is always absent). From these mutants we now have a time line of when the SC is necessary to maintain

423 pairing and recombination on the *X* chromosome and the autosomes. By comparing
424 these mutants, we can hypothesize that the *X* chromosome needs full-length SC earlier
425 in pachytene for proper maintenance of pairing and recombination while the autosomes
426 are likely capable of placing crossovers as late as mid pachytene resulting in a
427 centromere-proximal shift in crossovers where pairing is maintained (Fig 7).

428 In both *c(3)G*$^{cc\Delta 1}$ and *c(3)G*$^{cc\Delta 3}$ mutants, distal pairing of the *X* chromosome and
429 the autosomes was most strongly reduced. One likely explanation for this is that
430 normally the disassembly of the SC is initiated on the euchromatic chromosome arms
431 with the centromeric region being removed last. Since the loss of the SC in c*(3)G*$^{cc\Delta 1}$
432 and *c(3)G*$^{cc\Delta 3}$ mutants occurs in a manner similar to wild type SC disassembly, the distal
433 regions of the chromosome may be affected earlier and more strongly than the
434 centromere-proximal regions. The centromere-proximal region contains a large amount
435 of heterochromatin that could be mediating pairing interactions and stabilizing pairing in
436 the absence of the SC (Dernburg et al., 1998). Furthermore, our examination of
437 centromere pairing suggests that the centromeres are still paired (Fig 6.2) and could be
438 facilitating the centromere-proximal pairing. This idea is supported by the higher levels
439 of centromere-proximal pairing compared to distal pairing in *c(3)G*^{68} (Fig 6.1A).

440 Finally, we speculate that the ability of the c*(3)G*$^{cc\Delta 1}$ mutants to exhibit a
441 centromere-distal pairing defect that is more severe than the defect seen in *c(3)G*^{68}
442 mutants results from the residual proximal crossovers that do form in *c(3)G*$^{cc\Delta 1}$ mutants.
443 Previous work has shown that crossovers can preserve synapsis but only in their vicinity
444 (Maguire, 1985; Maguire and Riess, 1994). Perhaps the stresses that provoke
445 separation become more concentrated on the distal regions that lack crossovers. For

example, it is possible that the un-tethered distal regions could experience a higher mechanical stress due to nuclear movements than the pericentric regions containing a crossover. The lack of a strong pairing defect in *c(3)G*$^{cc\Delta 2}$ mutants is probably due to the persistence of full-length SC until mid pachytene. Together these data support a role for the SC in maintaining euchromatic pairing during early to mid prophase (Fig 7).

What causes the increase in centromere-proximal recombination events?

The autosomal increase in centromere-proximal crossovers displayed in these mutants mimics the interchromosomal effect (Crown et al., 2018; Joyce and McKim, 2009). The interchromosomal effect has been reported in flies that are heterozygous for chromosomes aberrations that suppress exchange in trans to a wild type chromosome (Lucchesi et al., 1976). Thus the absence of crossover formation on one chromosome promotes increased recombination on the other chromosomes, with more crossovers placed in the centromere-proximal regions (Crown et al., 2018; Joyce and McKim, 2009). The mechanism that controls the interchromsomal effect in balancer heterozygotes is poorly understood. It is possible that the interchromosomal effect is partially responsible for the increase in centromere-proximal crossovers in *c(3)G*$^{cc\Delta 1}$ and *c(3)G*$^{cc\Delta 3}$ mutants due to the loss of *X* chromosome recombination.

However, the interchromosomal effect cannot explain the increase in centromere-proximal recombination in *c(3)G*$^{cc\Delta 2}$ mutants since *X* recombination appears normal. Another explanation for the increase in centromere-proximal recombination events may be the premature loss of the SC at distal regions of the chromosome. It is unknown how much of a role the SC plays in the repair of DSBs into crossover versus

non-crossover events. It is possible the SC must be present to interact with factors necessary for regulating the placement of crossovers. For example, Vilya, a pro-crossover factor, localizes to the SC and DSBs prior to being recruited to recombination nodules (Lake et al., 2015). If DSB repair on the autosomes does not occur until early-mid pachytene and the SC is necessary for the determination of a crossover fate, it follows that distal loss of SC would result in a shift of crossover formation towards centromere-proximal regions where the SC is still present. This mechanism could also be increasing centromere-proximal recombination in *c(3)G*$^{cc\Delta 1}$ and *c(3)G*$^{cc\Delta 3}$ flies. Alternatively, SC-independent heterochromatic pairing may be holding the centromere-proximal region in close proximity allowing for crossing over in that region. In addition to interacting with pro-crossover factors the SC may be interacting with a currently unknown protein which regulates crossover placement differently on the *X* chromosome versus the autosomes.

Why is there a difference between the *X* chromosome and the autosomes?

This set of mutants represents a unique tool to investigate not only the temporal requirements of the SC but the differences in crossover placement between the *X* chromosome and the autosomes. Since *c(3)G*$^{cc\Delta 2}$ mutants do not display defects in *X* chromosome recombination we conclude that full-length SC in early-mid pachytene is necessary for *X* chromosome crossover placement (Fig 7). Examining autosomal recombination in all three mutants suggests that full-length SC is necessary in mid pachytene for proper crossover distribution on the autosomes (Fig 7). There are multiple

491 explanations for the recombination differences between the *X* chromosome and the
492 autosomes.

493 The first of these hypotheses is that there might exist a timing difference in either
494 synapsis or crossover placement between the *X* chromosome and the autosomes. Work
495 in *C. elegans* has provided evidence for timing differences between the sex
496 chromosomes and the autosomes. For example, the *X* chromosome initiates pre-
497 meiotic DNA replication later than the autosomes (Jaramillo-Lambert et al., 2007;
498 Mlynarczyk-Evans and Villeneuve, 2017). Additionally, in *C. elegans* the *X* chromosome
499 and the autosomes pair at the same time but synapsis of the *X* chromosome is delayed
500 compared to the autosomes (Mlynarczyk-Evans and Villeneuve, 2017). The timing of
501 when each chromosome is fully synapsed could be critical to ensure normal crossover
502 placement, and the premature disruption of synapsis may affect the activity of pro-
503 crossover factors. For example in *C. elegans*, the XND-1 protein is required for
504 genome-wide crossover placement and is important for normal rates of DSBs on the *X*
505 chromosome (Wagner et al., 2010). Currently, it is unknown in *Drosophila* if there are
506 differences in the timing of DSB repair or synapsis of the *X* chromosome as compared
507 to the autosomes, and our data suggest this as a possibility.

508 A second, but not mutually exclusive, explanation for the differences between the
509 chromosomes may be a structural one. The *X* chromosome is acrocentric (centromere
510 is near the end of the chromosome), while the autosomes are both metacentric
511 (centromere is near the center of the chromosome), and perhaps, these structural
512 differences mean that the *X* chromosome is more sensitive to loss of the SC. Our data
513 suggest that loss of SC maintenance disrupts the maintenance of euchromatic homolog

514 pairing more severely on the *X* chromosome than on the autosomes. It is unknown if
515 metacentric chromosomes are different in terms of synapsis and recombination as
516 compared to acrocentric chromosomes, and further investigation is needed to determine
517 if structural differences affect these processes.

518 It is clear from decades of research that the regulation of recombination requires
519 many factors and precise timing. Here we show that the SC plays a vital role in
520 maintaining homolog pairing and proper crossover distribution in *Drosophila* female
521 meiosis. Many differences between sex chromosomes and autosomes have been
522 documented in a multitude of organisms, and our data are consistent with these
523 differences extending into the processes that control chromosome pairing and
524 recombination. With this set of mutants, we have established a new system to examine
525 *X* chromosome and autosome biology in *Drosophila* meiosis that will allow future work
526 to unravel the mechanism behind meiotic chromosomal differences.

527

528 ## Materials and Methods

529 *Stocks*

530 *Drosophila* stocks were maintained on standard food at 24°C. Descriptions of genetic
531 markers and chromosomes can be found at http://www.flybase.org/. Wild type refers to
532 the genotype: *y w; +/+; +/+; sv$^{spa\text{-}pol}$*, unless stated otherwise. The key resource table
533 contains a list of all the fly stocks used in this manuscript.

534

535 *Construction of c(3)G$^{cc\Delta 1}$ mutants*

536 To aid in screening for *c(3)G*$^{cc\Delta 1}$ mutant flies, we incorporated a *piggyBac*
537 transposon carrying a *3xP3*-DsRed that expresses in the fly eye into the intron directly
538 downstream of the intended *c(3)G*$^{cc\Delta 1}$ deletion [intron 5 of *c(3)G*] in the homologous
539 repair template plasmid. Repair of the Cas9-induced DSB using the homologous repair
540 plasmid will insert the desired mutation and the *piggyBac* transposon into the genome at
541 the *c(3)G* locus. This allowed us to screen for the flies that undergo DSB repair off the
542 homologous repair plasmid by searching for those that express dsRed in the eyes.
543 Then, after isolation and confirmation of the desired *c(3)G* mutation, we excised the
544 *piggyBac* transposon by crossing in a transposase. This removed any potential effect
545 the *piggyBac* transposon may have on the expression of *c(3)G*.
546 The *piggyBac* transposon plasmid was constructed to have flanking *Aar*I and
547 *Sap*I restriction sites (Addgene 51434). We used PCR to obtain two fragments of *c(3)G*
548 from the *Drosophila* genome that flanked the position where the *piggyBac* would be
549 inserted and added in either an *Aar*I or *Sap*I restriction site. The ~2600-bp fragment
550 upstream of the *piggyBac* insertion site contained *Aar*I sites and was obtained using
551 these primers: Forward, tataCACCTGCattaCCGAcgctagtggctcctagagttcag; Reverse,
552 gcagCACCTGCgcggTTAAtgaaaaagaatttataagtcttaccattaggttatc. The ~1000-bp
553 fragment downstream of the *piggyBac* insertion site contained *Sap*I sites and was
554 obtained using these primers: Forward, gccgGCTCTTCNTAAccttttttctacaaaatgatttatt;
555 Reverse, gtatGCTCTTCNCGGtcatcaaaacatagtttagtatcg.
556 To insert these fragments into the *piggyBac* plasmid, the plasmid and the
557 downstream *Sap*I-containing PCR was digested with *Sap*I (also called *LguI* from
558 ThermoFisher, ER1931), phosphatase treated (Antarctic phosphatase, NEB M0289S),

559 and ligated together using T4 ligase (NEB, M0202S). Then, to make the *c(3)G*$^{cc\Delta 1}$
560 mutation, the upstream *Aar*I-containing PCR fragment was TOPO cloned using the Zero
561 Blunt TOPO kit (ThermoFisher, 451245) and cut using the restriction enzyme *HindIII*
562 (NEB, R0104S) to remove the 702-bp fragment from *c(3)G* creating the *c(3)G*$^{cc\Delta 1}$
563 mutation. The cut TOPO *AarI* plasmid was then phosphatase treated and ligated back
564 together to create the *c(3)G*$^{cc\Delta 1}$ deletion. Then, this plasmid was digested with AarI
565 (ThermoFisher ER1581) to generate a ~1900-bp fragment containing the *c(3)G*$^{cc\Delta 1}$
566 deletion, which was cloned into the *piggyBac* plasmid containing the downstream *Sap*I
567 *c(3)G* fragment. This created the *c(3)G*$^{cc\Delta 1}$ homologous repair template plasmid, which
568 was fully sequenced to ensure all cloning occurred in the correct direction (See Key
569 Resources for primers).

570 A CRISPR target sequence was selected from the flyCRISPR Optimal Target
571 Finder (http://tools.flycrispr.molbio.wisc.edu/targetFinder/). Only a single site upstream
572 of the *c(3)G*$^{cc\Delta 1}$ deletion was selected (AAAGCTTTGTTGGCCTGTATTGG) and
573 constructed into the pU6-BbsI-chiRNA guide RNA (gRNA) plasmid (Addgene 45946).
574 Sense (CTTCGAAAGCTTTGTTGGCCTCTAT) and antisense
575 (AAACATAGAGGCCAACAAAGCTTTC) oligonucleotides were ordered from IDT and
576 cloned into the gRNA plasmid as described by the flyCRISPR subcloning pU6-gRNA
577 protocol (http://flycrispr.molbio.wisc.edu/protocols/gRNA). After selection of the CRISPR
578 target sequence, three single nucleotide polymorphisms (SNPs) were made in the
579 CRISPR target sequence (the mutated bases are shown in bold:
580 ccaataga**a**gc**g**aa**t**aaagcttt) in the *c(3)G*$^{cc\Delta 1}$ homologous repair template plasmid to
581 prevent Cas9 from cutting this plasmid. These SNPs were made using the Quik Change

582 II XL Site-Directed Mutagenesis Kit (Agilent Technology, 200521). The gRNA and
583 *c(3)G*^{ccΔ1} homologous repair template plasmid were sent to Genetivision (Houston,
584 Texas) for injection into *y m[VASA-Cas9-3xGFP]ZH-2A-3xRFP w*^{1118}*/FM7c* flies (BLM
585 51323). Genetivision injected the gRNA plasmid at 250 ng/µl and the *c(3)G*^{ccΔ1}
586 homologous repair template at 500 ng/µl.
587 *c(3)G*^{ccΔ1} was isolated by crossing the G0 injected flies to *y w; Pr/TM3; sv*$^{spa\text{-}pol}$,
588 then the F1 progeny were screened for expression of dsRed in the fly eyes. Due to the
589 *VASA-Cas9* transgene also being marked with RFP, only F1 males could be screened
590 for CRIPSR insertion using dsRed expression. 15 G0 males were recovered from the
591 commercially injected embryos (Genetivision) and crossed to *y w; Pr/TM3; sv*$^{spa\text{-}pol}$. PCR
592 and Sanger sequencing were used to confirm that that male had repaired off the repair
593 template to incorporate the *c(3)G*^{ccΔ1} deletion mutation at the genomic *c(3)G* locus (See
594 Key Resources). This was done by using forward and reverse primers that were outside
595 of the 1kb both up and downstream repair sequence (See Key Resources). Following
596 removal of the *piggyBac,* we sequenced the entire *c(3)G* gene to confirm both the
597 precise excision of the transposon and that the only lesion in the gene was the desired
598 *c(3)G*^{ccΔ1} deletion mutation. Only one male was identified and was used to establish a
599 stock.
600
601 *Construction of c(3)G*^{ccΔ2} and *c(3)G*^{ccΔ3} *mutants*
602 A CRISPR target sequence was selected from the flyCRISPR Optimal Target Finder
603 (http://tools.flycrispr.molbio.wisc.edu/targetFinder/). Two guide RNAs were created for
604 *c(3)G*^{ccΔ2} and *c(3)G*^{ccΔ3} (guide 1 *c(3)G*^{ccΔ2}: GCTCAATGCGATC**T**TC**A**AGCTG**G**, guide 2

c(3)G$^{cc\Delta 2}$: GATTGACTGATCA**G**GC**A**AC**G**AG**G**, guide 1 *c(3)G*$^{cc\Delta 3}$: GCTCTTCCTG**A**TTGCTGCG**A**TG**G**, and guide 2 *c(3)G*$^{cc\Delta 3}$: TCTTGAACAAC**A**ATCTGTC**A**AG**G**) and constructed into the pU6-BbsI-chiRNA guide RNA (gRNA) plasmid (Addgene 45946). Sense and antisense oligonucleotides (guide 1 *c(3)G*$^{cc\Delta 2}$: CTTCGCTCAATGCGATCTTCAAGCTGG, AAACCCAGCTTGAAGATCGCATTGAGC; guide 2 *c(3)G*$^{cc\Delta 2}$: CTTCGATTGACTGATCAGGCAACGAGG, AAACCCTCGTTGCCTGATCAGTCAATC; guide 1 *c(3)G*$^{cc\Delta 3}$: CTTCGCTCTTCCTGATTGCTGCGATGG, AAACTCGCAGCAATCAGGAAGAGC; guide 2 *c(3)G*$^{cc\Delta 3}$: CTTCTCTTGAACAACAATCTGTCAAGG, AAACTGACAGATTGTTGTTCAAGAC) were ordered from IDT and cloned into the gRNA plasmid as described by the flyCRISPR subcloning pU6-gRNA protocol (http://flycrispr.molbio.wisc.edu/protocols/gRNA).

The homologous repair constructs were created using the NEBuilder HiFi DNA Kit (NEB, E5520S) and contained 1,000 bases upstream of the first guide RNA target Cas9 site, the *c(3)G* sequence with either 42 bp (*c(3)G*$^{cc\Delta 2}$) or 21 bp (*c(3)G*$^{cc\Delta 3}$) removed, and 1,000 bases downstream of the second guide RNA site. The PAM sequences in the *c(3)G* gene were mutated using the Quik Change II XL Site-Directed Mutagenesis Kit (Agilent Technology). The bases changed are in bold above. Additionally, a restriction site was engineered into the repair template, without creating coding changes, to aid in genotyping (*Spe*I for *c(3)G*$^{cc\Delta 2}$ and *Nhe*I for *c(3)G*$^{cc\Delta 3}$).

250 ng of each gRNA plasmid and 500 ng of the homologous repair template plasmid were injected (BestGene) into *y nosCas9* (on *X* chromosome, BDSC #54591). Potential CRISPR/Cas9 hits were screened with primers (See Key Resources), which

amplify a region spanning the deletion and were digested with either *Spe*I or *Nhe*I allowing for visualization of heterozygotes. Once a CRISPR/Cas9 insertion was identified, the entire *c(3)G* gene was sequenced to ensure the repair plasmid did not insert.

Nondisjunction and recombination assays

To assay recombination along the *X* chromosome, females of the genotypes: (1) $y^1\ sc^1\ cv^1\ v^1\ f^1\ y^+/y\ w;\ sv^{spa\text{-}pol}$; 2) $y^1\ sc^1\ cv^1\ v^1\ f^1\ y^+/y\ w;\ ru^1\ h^1\ Diap1^1\ st^1\ cu^1\ c(3)G^{cc\Delta1}\ ca^1;\ sv^{spa\text{-}pol}/+$; 3) $y^1\ sc^1\ cv^1\ v^1\ f^1\ y^+/y\ w;\ ru^1\ h^1\ Diap1^1\ st^1\ cu^1\ c(3)G^{cc\Delta2}\ ca^1;\ sv^{spa\text{-}pol}/+$; 4) $y^1\ sc^1\ cv^1\ v^1\ f^1\ y^+/y\ w;\ ru^1\ h^1\ Diap1^1\ st^1\ cu^1\ c(3)G^{cc\Delta3}\ ca^1;\ sv^{spa\text{-}pol}/+$) were crossed to $y^1\ sc^1\ cv^1\ v^1\ f^1\ car^1/B^SY$ males. For *X* recombination analysis, only the female progeny were analyzed for the intervals *sc-cv*, *cv-v, v-f, f-y+*.

To assay recombination along the *2nd* chromosome, females of the genotypes: 1) $y\ w/w;\ net^1\ dpp^{ho}\ dpy^{ov1}\ b^1\ pr^1\ cn^1/+;\ ru^1\ h^1\ Diap1^1\ st^1\ cu^1\ c(3)G^{cc\Delta1}\ ca^1/\ c(3)G^{cc\Delta1}\ ca^1;\ sv^{spa\text{-}pol}/+$; 2) $w^+/yw;\ net^1\ dpp^{ho}\ dpy^{ov1}\ b^1\ pr^1\ cn^1/+$ were crossed to $w^+/Y;\ net^1\ dpp^{ho}\ dpy^{ov1}\ b^1\ pr^1\ cn^1$ males. For *2nd* recombination analysis, only the female progeny were analyzed for the intervals *net-dpp, dpp-dpy, dpy-b, b-pr, pr-cn.*

To assay recombination frequency along the *3rd* chromosome females of the following genotypes: 1) $y\ w/\ w^+;\ ru^1\ h^1\ Diap1^1\ st^1\ cu^1\ sr^1\ e^s\ ca^1/+$; 2) $y\ w/\ w^+;\ ru^1\ h^1\ Diap1^1\ st^1\ cu^1\ c(3)G^{cc\Delta1}\ ca^1/\ c(3)G^{cc\Delta1}\ ca^1;\ sv^{spa\text{-}pol}/+$; 3) $y\ w/w^+;\ ru^1\ h^1\ Diap1^1\ st^1\ cu^1\ c(3)G^{cc\Delta2}\ ca^1/\ c(3)G^{cc\Delta2}\ ca^1;\ sv^{spa\text{-}pol}/+$; 4) $y\ w/w^+;\ ru^1\ h^1\ Diap1^1\ st^1\ cu^1\ c(3)G^{cc\Delta3}\ ca^1/\ c(3)G^{cc\Delta3}\ ca^1;\ sv^{spa\text{-}pol}/+$; were crossed to $w+/Y;\ ru^1\ h^1\ Diap1^1\ st^1\ cu^1\ sr^1\ e^s\ ca^1$ males.

For *3rd* recombination analysis, only the female progeny were analyzed for the intervals *ru-h, h-st, st-cu.*

To measure the rate of both *X* and *4th* chromosome nondisjunction single virgin females of the indicated genotype were mated to multiple *X^Y, In(1)EN, v f B; C(4)RM, ci ey^R* males. Calculations to determine the percentage of *X* and *4th* chromosome nondisjunction were performed as previously described (Hawley et al., 1992; Zitron and Hawley, 1989).

Immunostaining of whole-mount ovaries

Germarium preparation for whole-mount immunofluorescence was modified from the protocol described in (Lake et al., 2015), with dissections performed in PBS with 0.1% Tween (PBST). Primary antibodies used included affinity-purified rabbit anti-Corolla (1:2000), mouse anti-C(3)G 1A8-1G2, 5G4-1F1, and 1G5-2F7 (all at 1:500), rabbit anti-histone H2AVD pS137 (1:500) (Rockland Inc.), mouse anti-γH2AV (1:1000) (Iowa Hybridoma Bank), rat anti-CID (used at 1:3000; gift from Claudio Sunkel), and rat anti-CID (1:500) (Hanlon et al., 2018). All secondary antibodies were used at 1:500, and the secondary antibodies used were Alexa Fluor 488 goat anti-mouse (ThermoFisher, A11001), Alexa Fluor 555 goat anti-mouse (ThermoFisher, A21422), Alexa Fluor 647 goat anti-mouse (ThermoFisher, A21235), Alexa Fluor 488 goat anti-rabbit (ThermoFisher, A11008), Alexa Fluor 555 goat anti-rabbit (ThermoFisher, A21428), Alexa Fluor 647 goat anti-rat (ThermoFisher, A21434), and Alexa Fluor 555 goat anti-rat (ThermoFisher, A21247).

672 For STED imaging, samples were imaged with 100x, N.A 1.40 oil. objective on a
673 Lieca SP8 Gated STED microscope. Alexa Flour 647 labeled secondary was imaged
674 with a pulsed white light (80 MHz) tuned to 647 nm; Alexa Fluor 594 labelled secondary
675 was imaged with the same white laser tuned at 594 nm. Both secondaries were
676 depleted with a pulsed STED 775 nm laser with 80-90% maximum power. All images
677 were acquired in 2D mode to improve lateral resolution, and each image was averaged
678 8 times in line average mode. The emission photons were collected with an internal
679 Leica HyD hybrid detector with a time gate between 1-6 ns. Raw STED images were
680 deconvolved with the STED module in Huygens professional deconvolution software
681 (version 14.10; Scientific Volume Imaging). A theoretical estimated point spread
682 function was calculated from the raw images metadata. We used the default setting to
683 process images, but the background was measured from raw data, also the signal to
684 noise was set in the range of 15-20 depending on the signal intensity.
685
686 *Fluorescent in situ hybridization*
687 FISH probes were designed from bacterial artificial chromosomes (BACs) obtained from
688 the Children's Hospital Oakland Research Institute (CHORI;
689 http://bacpacresources.org/library.php?id=30). The following BACs were used: for *2L*
690 RP98-28O9 (polytene band 22A2-22A4), RP98-43K24 (polytene band 32E2-32F2),
691 RP98-7D17 (polytene band 38E4-38F4); for *3L* RP98-2N23 (polytene band 61D-61E),
692 RP98-26C20 (polytene band 69B1-69C2), RP98-3J2 (polytene band 77F5-78B1); for
693 the *X* RP98-3D13 (polytene band 3C3-3C7), RP98-9H1 (polytene band 15C1-15D6). To
694 make the FISH probes, the BACs were PCR amplified using the Illustra GenomiPhi V2

DNA Amplification Kit (GE 25-6600-30). The concentration of the BAC DNA was determined using a Quibit and 10 ng BAC DNA was used per amplification reaction. The amplification reaction was performed via kit protocol. Next, the amplified BAC was restriction enzyme digested using *AluI* (NEB R137S), *HaeII* (NEB R107S), *MseI* (NEB R0525S), *RsaI* (NEB R0167S), *MboI* (NEB R0147S) and *MspI* (NEB R0106S). Following the digestion, the DNA was ethanol precipitated with glycogen (ThermoFisher, 10814010). The precipitated DNA was resuspended in the labeling buffer from the ULYSIS Nucleic Acid Labeling Kits (ThermoFisher – AF647 kit, U21660; AF546 kit, U21652). To label the DNA with AF647 or AF546, the protocol in the ULYSIS Nucleic Acid Labeling Kits was used with 10 µL of the digested BAC DNA. The unreacted dyes were removed from the labeling reaction using Centri-Sep Columns (Princeton Separation, CS-900).

FISH with immunohistochemistry was performed as previously described (Christophorou et al., 2013), using anti-mouse C(3)G 1A8-1G2, 5G4-1F1, and 1G5-2F7 (all at 1:500) and mouse anti-Orb antibodies 4H8 and 6H4 (1:20 each)(Developmental Studies Hybridoma Bank, Iowa). C(3)G staining was used to identify meiotic nuclei in early, early-mid or mid pachytene with the exception that in *c(3)G*$^{cc\Delta 3}$ mutants mid pachytene oocytes were identified using Orb staining due to the lack of SC present. To measure the 3D distance between the FISH probe foci, a custom ImageJ plug-in ("3D jru v1") was used with a slice spacing of 0.20 and pixel spacing of 0.06370 (available at http://research.stowers.org/imagejplugins). A locus was considered paired if the distance between the FISH probe foci was <0.75 µm and unpaired if the distanced between the FISH probe foci was ≥0.75 µm.

718

719 *Imaging and image analysis*

720 Except for the STED imaging (see below), all images were acquired on an inverted
721 DeltaVision microscopy system (GE Healthcare) with an Olympus 100x Objective
722 (UPlanSApo 100x NA 1.40) and a high-resolution CCD camera or an Applied Precision
723 OMX Blaze microscope (Issaquah, WA, USA) equipped with a PCO Edge sCMOS
724 camera. Images were deconvolved (DeltaVision and OMX) and reconstruction was
725 performed (OMX) using SoftWoRx v. 6.5 software (Applied Precision/GE Healthcare)
726 following Applied Precision protocols. Images were cropped and brightness and
727 contrast was slightly adjusted using ImageJ.

728

729 *Length measurements for the synaptonemal complex*
730
731 These were performed utilizing custom macros in ImageJ (NIH, Bethesda, MD). C(3)G
732 signals corresponding to roughly a single nucleus were traced approximately in 3D as
733 follows. Firstly, structured illumination images were scaled in x and y by 4 with bilinear
734 interpolation. Then they were blurred in x and y with a standard deviation of 8 pixels (80
735 nm). Next a rolling ball background with a radius of 50 pixels was subtracted. The
736 resulting 3D images were thresholded at 25% of their maximum intensity to create a
737 mask encompassing the synaptonemal complex fibers. Objects containing less than
738 500 voxels in 3D corresponded to noise in the image and were removed. Finally, the
739 images were skeletonized in 3D using the 3D skeletonize plugin (based on (Lee et al.,
740 1994), CVGIP: Graphical Models and Image Processing) to create single pixel traces of
741 the SC in three dimensions. These were dilated once to close single pixel gaps and

each 3D fiber volume was measured in voxel units for presentation. Single outliers were tested for and removed with the Grubbs test at a 1% confidence level. Statistical assessment of volume differences was accomplished with a two tailed T test.

Line Profile Analysis of STED data

Following the profile averaging approach described in (Cahoon et al., 2017) we assessed the width of the SC. Briefly, single slice cross sectional intensity profiles were generated from manually drawn lines across regions of the SC that appeared to be flat in the z dimension (traveled along the selected plane for a substantial distance). We then aligned all of these profiles (as well as the Corolla signals where present) so that the midpoint between the C(3)G C-termini was at 0. Then, the profiles were averaged to create low noise average profile distributions. A standard t-test was used for statistical comparisons between the *c(3)G*$^{cc\Delta 1}$ and wild type, the mean and standard error of the mean (SEM) were reported.

Data and software availability

Primary data files for the figures in this paper are publicly accessible at www.stowers.org/research/publications/odr. For data analysis, the custom ImageJ plugins used are available at research.stowers.org/imagejplugins/zipped_plugins.html.

Acknowledgements

We thank Claudio Sunkel for antibodies; past and present members of the Hawley lab for helpful discussion and comments on this manuscript; and Angela Miller for editorial

765 and figure preparation assistance. R.S.H. is an American Cancer Society Research
766 Professor.

767

768 References

769 Anderson, L.K., Royer, S.M., Page, S.L., McKim, K.S., Lai, A., Lilly, M.A., Hawley, R.S.,
770 2005. Juxtaposition of C(2)M and the transverse filament protein C(3)G within the
771 central region of Drosophila synaptonemal complex. Proc. Natl. Acad. Sci. U. S. A.
772 102, 4482–7. https://doi.org/10.1073/pnas.0500172102
773 Ashburner, M., Golic, K., Hawley, R., 2005. Chromosomes and position effect
774 variegation. In Drosophila: A laboratory handbook, 2nd ed., C. ed. Cold Spring
775 Harbor Laboratory Press, Cold Spring Harbor, NY.
776 Baker, B.S., Hall, J.C., 1976. Meiotic mutants: genic control of meiotic recombination
777 and chromosome segregation. Genet. Biol. Drosoph. Vol. 1a, 351–434.
778 Berchowitz, L., Copenhaver, G., 2010. Genetic Interference: Dont Stand So Close to
779 Me. Curr. Genomics 11, 91–102. https://doi.org/10.2174/138920210790886835
780 Cahoon, C.K., Hawley, R.S., 2016. Regulating the construction and demolition of the
781 synaptonemal complex. Nat. Struct. Mol. Biol. 23, 369–377.
782 https://doi.org/10.1038/nsmb.3208
783 Cahoon, C.K., Yu, Z., Wang, Y., Guo, F., Unruh, J.R., Slaughter, B.D., Hawley, R.S.,
784 2017. Superresolution expansion microscopy reveals the three-dimensional
785 organization of the Drosophila synaptonemal complex. Proc. Natl. Acad. Sci. U. S.
786 A. 114, E6857–E6866. https://doi.org/10.1073/pnas.1705623114
787 Christophorou, N., Rubin, T., Huynh, J.-R., 2013. Synaptonemal Complex Components

788 Promote Centromere Pairing in Pre-meiotic Germ Cells. PLoS Genet. 9, e1004012.
789 https://doi.org/10.1371/journal.pgen.1004012
790 Collins, K.A., Unruh, J.R., Slaughter, B.D., Yu, Z., Lake, C.M., Nielsen, R.J., Box, K.S.,
791 Miller, D.E., Blumenstiel, J.P., Perera, A.G., Malanowski, K.E., Hawley, R.S., 2014.
792 Corolla Is a novel protein that contributes to the architecture of the synaptonemal
793 complex of Drosophila. Genetics 198.
794 Crown, K.N., Miller, D.E., Sekelsky, J., Hawley, R.S., 2018. Local Inversion
795 Heterozygosity Alters Recombination throughout the Genome. Curr. Biol. 28.
796 https://doi.org/10.1016/j.cub.2018.07.004
797 Dernburg, A.F., McDonald, K., Moulder, G., Barstead, R., Dresser, M., Villeneuve, A.M.,
798 1998. Meiotic Recombination in C. elegans Initiates by a Conserved Mechanism
799 and Is Dispensable for Homologous Chromosome Synapsis. Cell 94, 387–398.
800 https://doi.org/10.1016/S0092-8674(00)81481-6
801 Gladstone, M.N., Obeso, D., Chuong, H., Dawson, D.S., 2009. The synaptonemal
802 complex protein Zip1 promotes bi-orientation of centromeres at meiosis I. PLoS
803 Genet. 5, e1000771. https://doi.org/10.1371/journal.pgen.1000771
804 Gong, W.J., McKim, K.S., Hawley, R.S., 2005. All Paired Up with No Place to Go:
805 Pairing, Synapsis, and DSB Formation in a Balancer Heterozygote. PLoS Genet. 1,
806 e67. https://doi.org/10.1371/journal.pgen.0010067
807 Hall, J.C., 1972. CHROMOSOME SEGREGATION INFLUENCED BY TWO ALLELES
808 OF THE MEIOTIC MUTANT c(3)G IN DROSOPHILA MELANOGASTER. Genetics
809 71.
810 Hanlon, S.L., Miller, D.E., Eche, S., Hawley, R.S., 2018. Origin, Composition, and

811 Structure of the Supernumerary B Chromosome of Drosophila melanogaster.
812 Genetics 210, 1197–1212. https://doi.org/10.1534/genetics.118.301478
813 Hassold, T., Hall, H., Hunt, P., 2007. The origin of human aneuploidy: where we have
814 been, where we are going. Hum. Mol. Genet. 16, R203–R208.
815 https://doi.org/10.1093/hmg/ddm243
816 Hawley, R.S., Irick, H., Haddox, D.A., Whitley, M.D., Arbel, T., Jang, J., McKim, K.,
817 Zitron, A.E., New, C., Childs, G., Lohe, A., 1992. There are two mechanisms of
818 achiasmate segregation inDrosophila females, one of which requires
819 heterochromatic homology. Dev. Genet. 13, 440–467.
820 https://doi.org/10.1002/dvg.1020130608
821 Hughes, S.E., Miller, D.E., Miller, A.L., Hawley, R.S., 2018. Female Meiosis: Synapsis,
822 Recombination, and Segregation in Drosophila melanogaster. Genetics 208, 875–
823 908. https://doi.org/10.1534/genetics.117.300081
824 Jaramillo-Lambert, A., Ellefson, M., Villeneuve, A.M., Engebrecht, J., 2007. Differential
825 timing of S phases, X chromosome replication, and meiotic prophase in the C.
826 elegans germ line. Dev. Biol. 308, 206–21.
827 https://doi.org/10.1016/j.ydbio.2007.05.019
828 Jeffress, J.K., Page, S.L., Royer, S.M., Belden, E.D., Blumenstiel, J.P., Anderson, L.K.,
829 Hawley, R.S., 2007. The Formation of the Central Element of the Synaptonemal
830 Complex May Occur by Multiple Mechanisms: The Roles of the N- and C-Terminal
831 Domains of the Drosophila C(3)G Protein in Mediating Synapsis and
832 Recombination. Genetics 177, 2445–2456.
833 https://doi.org/10.1534/genetics.107.078717

834 Jordan, P.W., Karppinen, J., Handel, M.A., 2012. Polo-like kinase is required for
835 synaptonemal complex disassembly and phosphorylation in mouse spermatocytes.
836 J. Cell Sci. 125, 5061–5072. https://doi.org/10.1242/jcs.105015
837 Joyce, E.F., Apostolopoulos, N., Beliveau, B.J., Wu, C. -tin., 2013. Germline Progenitors
838 Escape the Widespread Phenomenon of Homolog Pairing during Drosophila
839 Development. PLoS Genet. 9, e1004013.
840 https://doi.org/10.1371/journal.pgen.1004013
841 Joyce, E.F., McKim, K.S., 2009. Drosophila PCH2 is required for a pachytene
842 checkpoint that monitors double-strand-break-independent events leading to
843 meiotic crossover formation. Genetics 181, 39–51.
844 https://doi.org/10.1534/genetics.108.093112
845 Keeney, S., Giroux, C.N., Kleckner, N., 1997. Meiosis-specific DNA double-strand
846 breaks are catalyzed by Spo11, a member of a widely conserved protein family.
847 Cell 88, 375–84.
848 Krishnan, B., Thomas, S.E., Yan, R., Yamada, H., Zhulin, I.B., McKee, B.D., 2014.
849 *Sisters Unbound* Is Required for Meiotic Centromeric Cohesion in *Drosophila*
850 *melanogaster*. Genetics 198, 947–965.
851 https://doi.org/10.1534/genetics.114.166009
852 Lake, C.M., Holsclaw, J.K., Bellendir, S.P., Sekelsky, J., Hawley, R.S., 2013. The
853 development of a monoclonal antibody recognizing the Drosophila melanogaster
854 phosphorylated histone H2A variant (γ-H2AV). G3 (Bethesda). 3, 1539–43.
855 https://doi.org/10.1534/g3.113.006833
856 Lake, C.M., Nielsen, R.J., Guo, F., Unruh, J.R., Slaughter, B.D., Hawley, R.S., 2015.

857 Vilya, a component of the recombination nodule, is required for meiotic double-
858 strand break formation in Drosophila. Elife 4. https://doi.org/10.7554/eLife.08287
859 Lee, T.C., Kashyap, R.L., Chu, C.N., 1994. Building Skeleton Models via 3-D Medial
860 Surface Axis Thinning Algorithms. CVGIP Graph. Model. Image Process. 56, 462–
861 478. https://doi.org/10.1006/CGIP.1994.1042
862 Libuda, D.E., Uzawa, S., Meyer, B.J., Villeneuve, A.M., 2013. Meiotic chromosome
863 structures constrain and respond to designation of crossover sites. Nature 502,
864 703–6. https://doi.org/10.1038/nature12577
865 Lindsley, D.L., Sandler, L., Counce, S.J., Chandley, A.C., Lewis, K.R., 1977. The
866 Genetic Analysis of Meiosis in Female Drosophila melanogaster [and Discussion].
867 Philos. Trans. R. Soc. B Biol. Sci. 277, 295–312.
868 https://doi.org/10.1098/rstb.1977.0019
869 Lucchesi, J., Ashburner, M., Novitsaki, E., 1976. The genetics and biology of
870 Drosophila.
871 Lupas, A., Dyke, M. Van, Stock, J., 1991. Predicting coiled coils from protein
872 sequences. Science (80-.). 252, 1162–1164.
873 https://doi.org/10.1126/SCIENCE.252.5009.1162
874 Lupas, A.N., Bassler, J., 2017. Coiled Coils - A Model System for the 21st Century.
875 Trends Biochem. Sci. 42, 130–140. https://doi.org/10.1016/j.tibs.2016.10.007
876 Maguire, M.P., 1985. Crossover frequencies within paracentric inversions in maize: the
877 implications for homologue pairing models. Genet. Res. 46, 273–8.
878 Maguire, M.P., Riess, R.W., 1994. The relationship of homologous synapsis and
879 crossing over in a maize inversion. Genetics 137, 281–8.

880 Manheim, E.A., McKim, K.S., 2003. The Synaptonemal complex component C(2)M
881 regulates meiotic crossing over in Drosophila. Curr. Biol. 13, 276–85.
882 McKim, K.S., Hayashi-Hagihara, A., 1998. mei-W68 in Drosophila melanogaster
883 encodes a Spo11 homolog: evidence that the mechanism for initiating meiotic
884 recombination is conserved. Genes Dev. 12, 2932–2942.
885 https://doi.org/10.1101/gad.12.18.2932
886 Mehrotra, S., McKim, K.S., 2006. Temporal Analysis of Meiotic DNA Double-Strand
887 Break Formation and Repair in Drosophila Females. PLoS Genet. 2, e200.
888 https://doi.org/10.1371/journal.pgen.0020200
889 Miller, D.E., Smith, C.B., Kazemi, N.Y., Cockrell, A.J., Arvanitakis, A. V., Blumenstiel,
890 J.P., Jaspersen, S.L., Hawley, R.S., 2016. Whole-Genome Analysis of Individual
891 Meiotic Events in *Drosophila melanogaster* Reveals That Noncrossover Gene
892 Conversions Are Insensitive to Interference and the Centromere Effect. Genetics
893 203, 159–171. https://doi.org/10.1534/genetics.115.186486
894 Miller, D.E., Takeo, S., Nandanan, K., Paulson, A., Gogol, M.M., Noll, A.C., Perera,
895 A.G., Walton, K.N., Gilliland, W.D., Li, H., Staehling, K.K., Blumenstiel, J.P.,
896 Hawley, R.S., 2012. A Whole-Chromosome Analysis of Meiotic Recombination in
897 Drosophila melanogaster. G3 (Bethesda). 2, 249–60.
898 https://doi.org/10.1534/g3.111.001396
899 Mlynarczyk-Evans, S., Villeneuve, A.M., 2017. Time-Course Analysis of Early Meiotic
900 Prophase Events Informs Mechanisms of Homolog Pairing and Synapsis in
901 Caenorhabditis elegans. Genetics 207, 103–114.
902 https://doi.org/10.1534/genetics.117.204172

903 Nadarajan, S., Lambert, T.J., Altendorfer, E., Gao, J., Blower, M.D., Waters, J.C.,
904 Colaiácovo, M.P., 2017. Polo-like kinase-dependent phosphorylation of the
905 synaptonemal complex protein SYP-4 regulates double-strand break formation
906 through a negative feedback loop. Elife 6. https://doi.org/10.7554/eLife.23437
907 Nicklas, R.B., 1974. CHROMOSOME SEGREGATION MECHANISMS. Genetics 78.
908 Page, S., Nielsen, R.J., Teeter, K., Lake, C.M., Ong, S., Wright, K.R., Dean, K.L., Agne,
909 D., Gilliland, W.D., Hawley, R.S., 2007. A germline clone screen for meiotic
910 mutants in Drosophila melanogaster. Fly (Austin). 1, 172–181.
911 https://doi.org/10.4161/fly.4720
912 Page, S.L., Hawley, R.S., 2001. c(3)G encodes a Drosophila synaptonemal complex
913 protein. Genes Dev. 15, 3130–43. https://doi.org/10.1101/gad.935001
914 Page, S.L., Khetani, R.S., Lake, C.M., Nielsen, R.J., Jeffress, J.K., Warren, W.D.,
915 Bickel, S.E., Hawley, R.S., 2008. corona is required for higher-order assembly of
916 transverse filaments into full-length synaptonemal complex in Drosophila oocytes.
917 PLoS Genet. 4, e1000194. https://doi.org/10.1371/journal.pgen.1000194
918 Parry, D.M., Sandler, L., 1974. The genetic identification of a heterochromatic segment
919 on the X chromosome of Drosophila melanogaster. Genetics 77, 535–9.
920 Previato de Almeida, L., Evatt, J.M., Chuong, H.H., Kurdzo, E.L., Eyster, C.A.,
921 Gladstone, M.N., Gómez-H, L., Llano, E., Meyer, R., Pendas, A.M., Pezza, R.J.,
922 Dawson, D.S., 2019. Shugoshin protects centromere pairing and promotes
923 segregation of nonexchange partner chromosomes in meiosis. Proc. Natl. Acad.
924 Sci. 201902526. https://doi.org/10.1073/pnas.1902526116
925 Sato-Carlton, A., Nakamura-Tabuchi, C., Chartrand, S.K., Uchino, T., Carlton, P.M.,

926 2017. Phosphorylation of the synaptonemal complex protein SYP-1 promotes
927 meiotic chromosome segregation. J. Cell Biol. jcb.201707161.
928 https://doi.org/10.1083/jcb.201707161
929 Sherizen, D., Jang, J.K., Bhagat, R., Kato, N., McKim, K.S., 2005. Meiotic
930 recombination in Drosophila females depends on chromosome continuity between
931 genetically defined boundaries. Genetics 169, 767–81.
932 https://doi.org/10.1534/genetics.104.035824
933 Storlazzi, A., Xu, L., Schwacha, A., Kleckner, N., 1996. Synaptonemal complex (SC)
934 component Zip1 plays a role in meiotic recombination independent of SC
935 polymerization along the chromosomes. Proc. Natl. Acad. Sci. U. S. A. 93, 9043–8.
936 Szauter, P., 1984. An analysis of regional constraints on exchange in Drosophila
937 melanogaster using recombination-defective meiotic mutants. Genetics 106, 45–71.
938 Takeo, S., Lake, C.M., Morais-de-Sá, E., Sunkel, C.E., Hawley, R.S., 2011.
939 Synaptonemal complex-dependent centromeric clustering and the initiation of
940 synapsis in Drosophila oocytes. Curr. Biol. 21, 1845–51.
941 https://doi.org/10.1016/j.cub.2011.09.044
942 Tanneti, N.S., Landy, K., Joyce, E.F., McKim, K.S., 2011. A Pathway for Synapsis
943 Initiation during Zygotene in Drosophila Oocytes. Curr. Biol. 21, 1852–1857.
944 https://doi.org/10.1016/j.cub.2011.10.005
945 Tung, K.S., Roeder, G.S., 1998. Meiotic chromosome morphology and behavior in zip1
946 mutants of Saccharomyces cerevisiae. Genetics 149, 817–32.
947 Voelkel-Meiman, K., Cheng, S.-Y., Morehouse, S.J., MacQueen, A.J., 2016.
948 Synaptonemal Complex Proteins of Budding Yeast Define Reciprocal Roles in

MutSγ-Mediated Crossover Formation. Genetics 203, 1091–103. https://doi.org/10.1534/genetics.115.182923

Wagner, C.R., Kuervers, L., Baillie, D.L., Yanowitz, J.L., 2010. xnd-1 regulates the global recombination landscape in Caenorhabditis elegans. Nature 467, 839–43. https://doi.org/10.1038/nature09429

Yan, R., McKee, B.D., 2013. The cohesion protein SOLO associates with SMC1 and is required for synapsis, recombination, homolog bias and cohesion and pairing of centromeres in Drosophila Meiosis. PLoS Genet. 9, e1003637. https://doi.org/10.1371/journal.pgen.1003637

Zeng, Y., Li, H., Schweppe, N.M., Hawley, R.S., Gilliland, W.D., 2010. Statistical Analysis of Nondisjunction Assays in Drosophila. Genetics 186, 505–513. https://doi.org/10.1534/genetics.110.118778

Zickler, D., Kleckner, N., 2015. Recombination, pairing, and synapsis of homologs during meiosis. Cold Spring Harb. Perspect. Biol. 7, a016626. https://doi.org/10.1101/cshperspect.a016626

Zickler, D., Kleckner, N., 1999. Meiotic chromosomes: integrating structure and function. Annu. Rev. Genet. 33, 603–754. https://doi.org/10.1146/annurev.genet.33.1.603

Zitron, A.E., Hawley, R.S., 1989. The genetic analysis of distributive segregation in Drosophila melanogaster. I. Isolation and characterization of Aberrant X segregation (Axs), a mutation defective in chromosome partner choice. Genetics 122, 801–21.

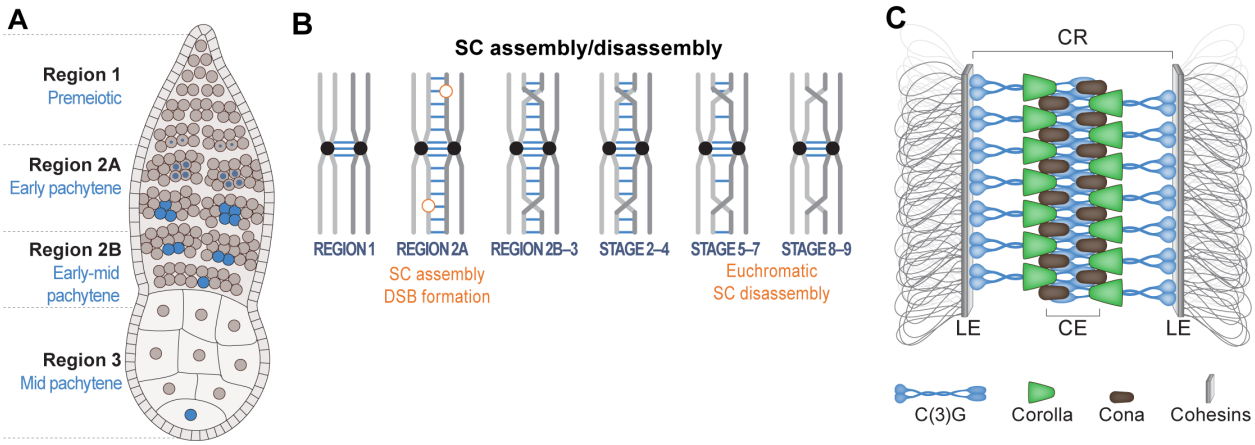

Figure 1: Schematic of early meiosis in *Drosophila*. (A) Diagram of a *Drosophila* germarium and SC formation (described in (Hughes et al., 2018)). At the anterior tip of the germarium, a germline stem cell divides asymmetrically to give rise to a cystoblast, which undergoes four mitotic divisions with incomplete cytokinesis to yield a 16-cell cyst. At region 2A (zygotene/early pachytene) up to 4 of the 16 cells in the cyst will enter meiosis and assemble the SC (SC represented by blue shading) to fully synapse the chromosomes. The oocyte selection process progresses in region 2B and is characterized by two nuclei (pro-oocytes) with full-length SC (early-mid pachytene) and is completed by region 3 (mid pachytene) with only one oocyte per cyst retaining full-length SC and all other nuclei having backed out of the meiotic program to become nurse cells. (B) Homologous chromosome pairing and SC assembly begin at the centromeres (represented as black dots on the chromosomes) during the mitotic divisions in region 1 (Christophorou et al., 2013; Joyce et al., 2013). In region 2A (early pachytene) the SC (represented by blue lines) is assembled along the chromosome arms and DSBs form (orange circles). The SC is maintained along chromosome arms

990 until stage 5-7 (late pachytene), when SC disassembly occurs at multiple regions along
991 the chromosome arms. The SC persists at the centromeres into stages 8–9 (mid
992 prophase)(Takeo et al., 2011; Tanneti et al., 2011). (C) Model of the *Drosophila* SC
993 showing the transverse filament protein C(3)G (blue), the central region (CR) protein
994 Corolla (green), the central element protein CONA (black), and the lateral
995 element/cohesin proteins (grey) connected to chromatin loops (adapted from (Hughes
996 et al., 2018)).
997
998
999

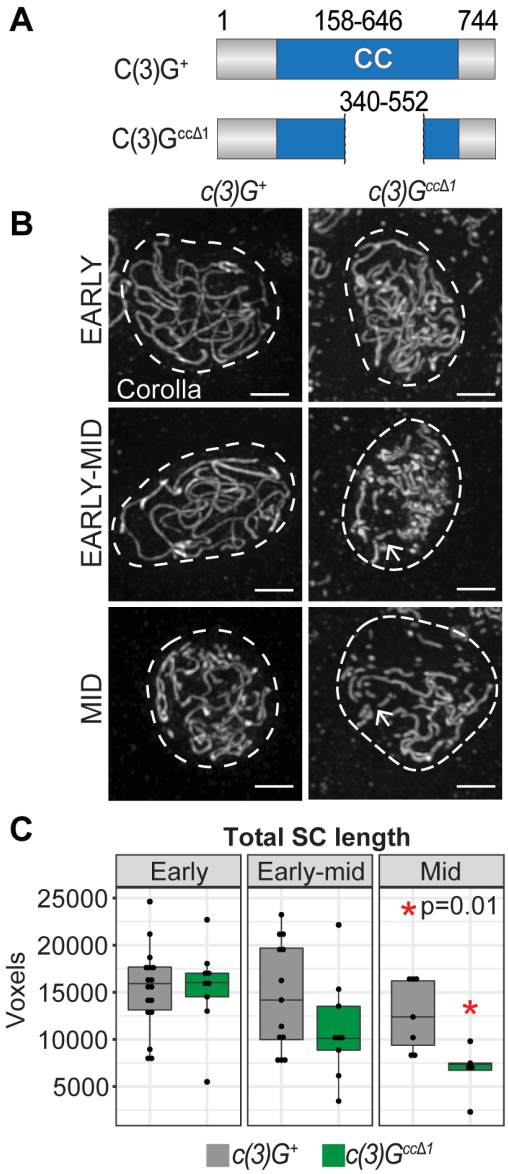

Figure 2: In-frame deletion of part of the large coiled-coil region of C(3)G leads to a failure to maintain SC. (A) The *c(3)G*$^{cc\Delta 1}$ deletion removes the amino acids 340–552 from the coiled-coil (CC) domain of C(3)G. The predicted protein CC is in blue (based on COILs software (Lupas et al., 1991)). (B) Images showing localization of the SC protein Corolla in *c(3)G*$^{+}$ and *c(3)G*$^{cc\Delta 1}$ nuclei from early pachytene (region 2A) to mid pachytene (region 3). Dotted lines indicate the location of the nucleus as defined by DAPI staining (not shown). Arrowheads indicate discontinuities in the SC. Scale bars, 2

1008 μm. (C) Quantification of the total track length of C(3)G-positive SC in nuclei from early,

1009 early-mid and mid pachytene using skeleton analysis (See Methods). *p=0.01 by t-test,

1010 *c(3)G*$^{+}$: N=17 (early), N=13 (early-mid), and N=7 (mid); *c(3)G*$^{cc\Delta 1}$: N=9 (early), N=9

1011 (early-mid), and N=5 (mid).

1012

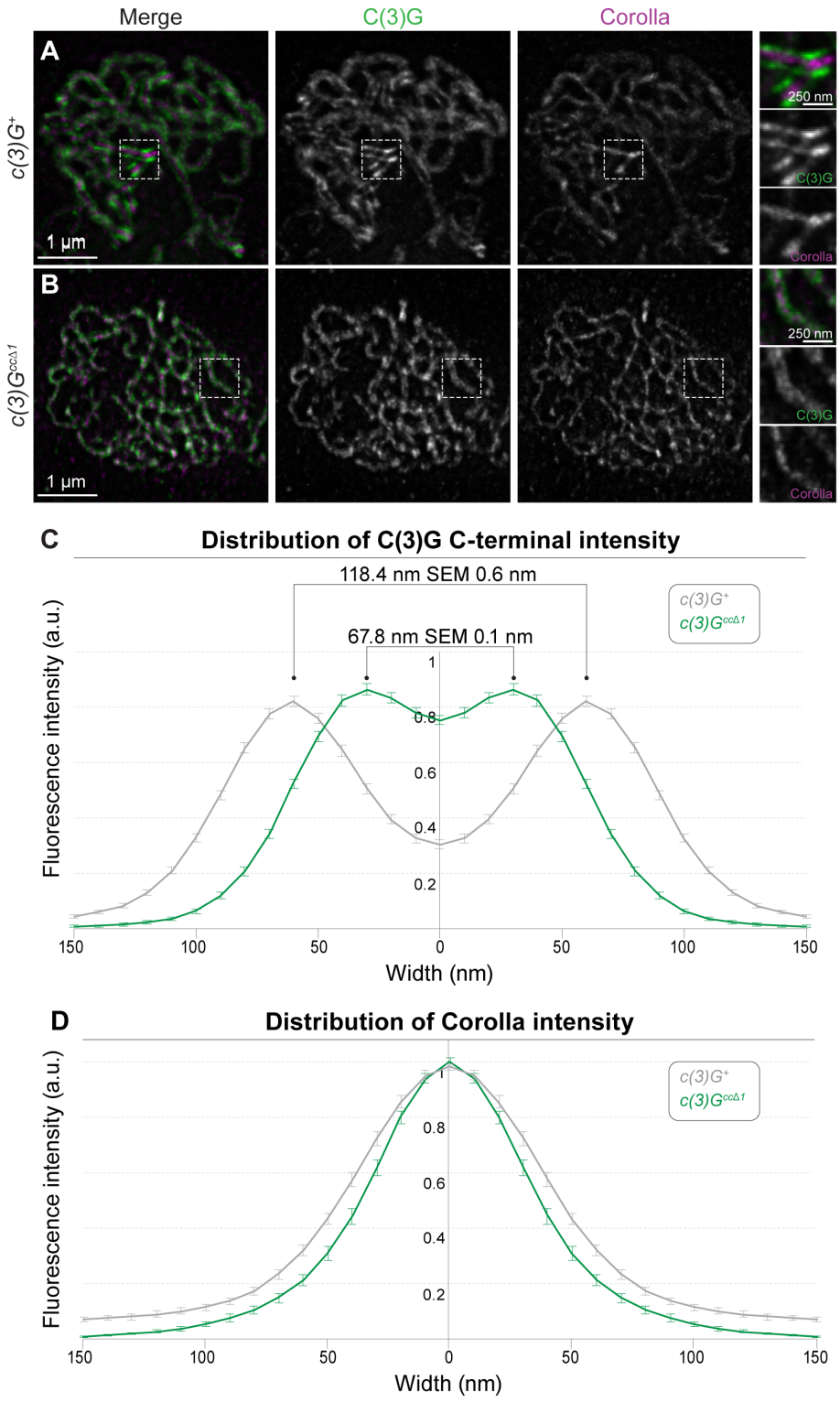

1013

1014 **Figure 2- figure supplement 1: Width of SC is reduced, but the tripartite structure**

1015 **is maintained, in *c(3)G*$^{cc\Delta 1}$ mutants in early pachytene.** STED images of early

pachytene nuclei with the C-terminus of C(3)G (green) and Corolla (magenta) labeled in *c(3)G*$^{+}$ (A) and *c(3)G*^{ccΔ1} mutants (B). (C)The average distribution of the distance between the two C-terminal C(3)G tracks is shown based on a line profile analysis of STED data in each genotype (see Methods). The quantification resulted in an average width of 118.4 nm ± 0.6 nm (SEM) in wild type and 67.8 nm ± 0.1 nm (SEM) in *c(3)G*^{ccΔ1} mutants. (D) The average distribution of the Corolla signal based on a line profile analysis of STED data in each genotype. The average distribution was generated by averaging 46 line profiles from 8 wild type nuclei and 35 line profiles from 12 *c(3)G*^{ccΔ1} nuclei.

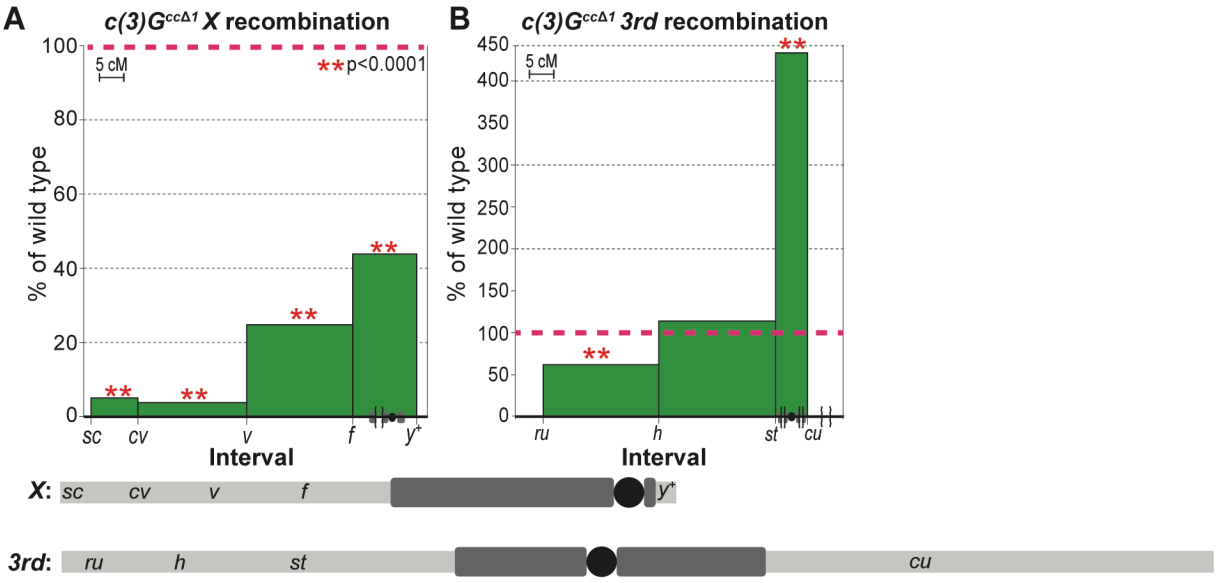

Figure 3: *c(3)G*^{ccΔ1} mutants exhibit chromosome-specific defects in recombination. Recombination in c*(3)G*^{ccΔ1} females on the *X* chromosome (A) and the *3rd* chromosome (B) are plotted with percent of wild type on the y-axis vs chromosome location (in cM) on the x-axis. Brackets along x-axis indicate truncation of that region of the chromosome. The red dotted line marks wild type levels of recombination and is set at 100%. P-values obtained using a Fisher's exact test (see Table 1,2 for N values). See Methods for the recessive markers used to assay recombination. For reference, below each chart is a diagram of the corresponding chromosome being analyzed displaying the relative cytological positions of the recombination markers and the approximate amounts of pericentromeric heterochromatin estimated from (Ashburner et al., 2005) (the black circle represents the centromere).

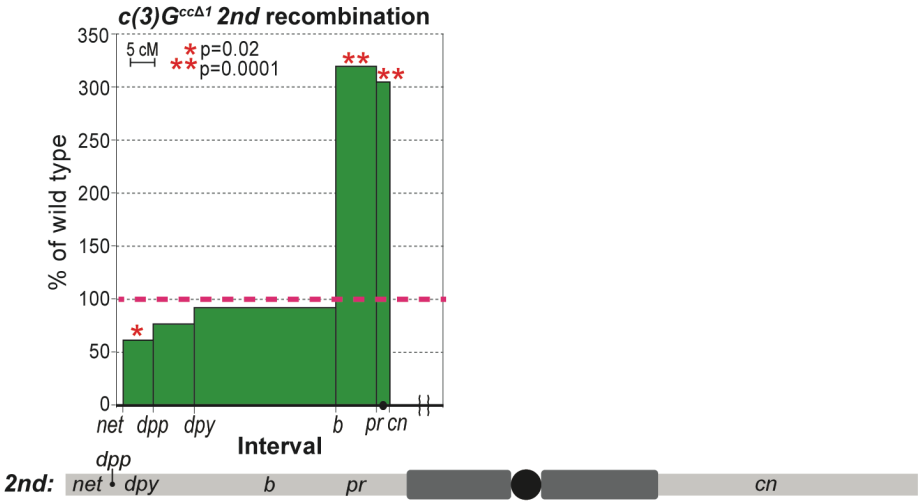

Figure 3- figure supplement 1: *c(3)G*^{ccΔ1} mutants exhibit recombination defects on the *2nd* chromosome. Recombination in *c(3)G*^{ccΔ1} mutants on the *2nd* chromosome plotted with percent of wild type on the y-axis vs chromosome location (in cM) on the x-axis. Brackets along x-axis indicate truncation of that region of the chromosome. The red dotted line marks wild type levels of recombination and is set to 100%. See Methods for the recessive markers used to assay recombination. P-values obtained using a Fisher's exact test (see Table 3 for N values). For reference, below each chart is a diagram of the corresponding chromosome being analyzed displaying the relative cytological positions of the recombination markers and the approximate amounts of pericentromeric heterochromatin estimated from (Ashburner et al., 2005) (the black circle represents the centromere).

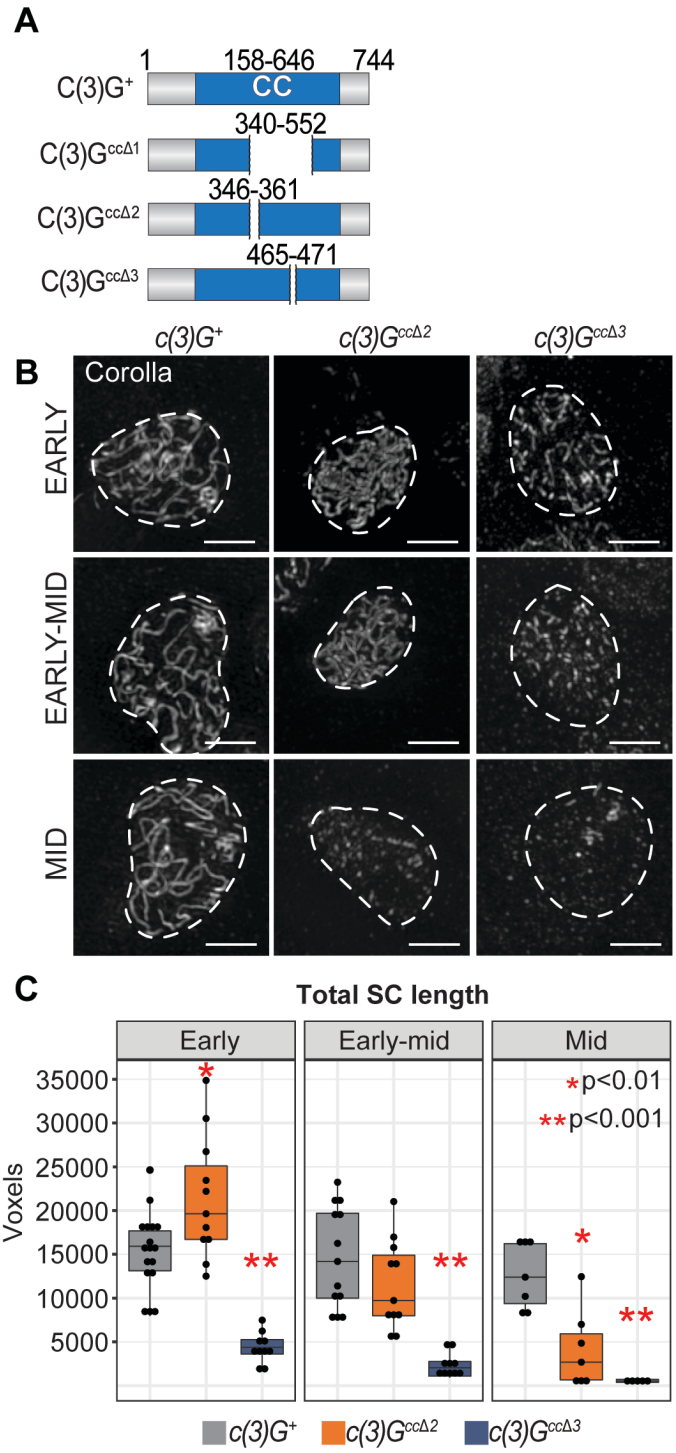

Figure 4: Two smaller in-frame deletions within the putative *c(3)G* coiled-coil region cause varying levels of SC defects. (A) Diagrams of the C(3)G^{+}, C(3)G^{ccΔ1}, C(3)G^{ccΔ2} and C(3)G^{ccΔ3} coding regions. (B) Images showing localization of the SC

protein Corolla in *c(3)G*$^{+}$, *c(3)G*$^{cc\Delta 2}$, and *c(3)G*$^{cc\Delta 3}$ mutants from early pachytene (region 2A) to mid pachytene (region 3). Dotted lines indicate the location of the nucleus as defined by DAPI staining (not shown). Scale bars, 2 μm. (C) Quantification of the total length of C(3)G positive SC in nuclei from early, early-mid and mid pachytene using skeleton analysis (See Methods). *c(3)G*$^{+}$ controls are the same ones used in Fig 2. *p<.01 and **p<.001 by t-test. *c(3)G*$^{cc\Delta 2}$: N=11 (early), N=11 (early-mid), and N=7 (mid); *c(3)G*$^{cc\Delta 3}$: N=10 (early), N=10 (early-mid), and N=5 (mid).

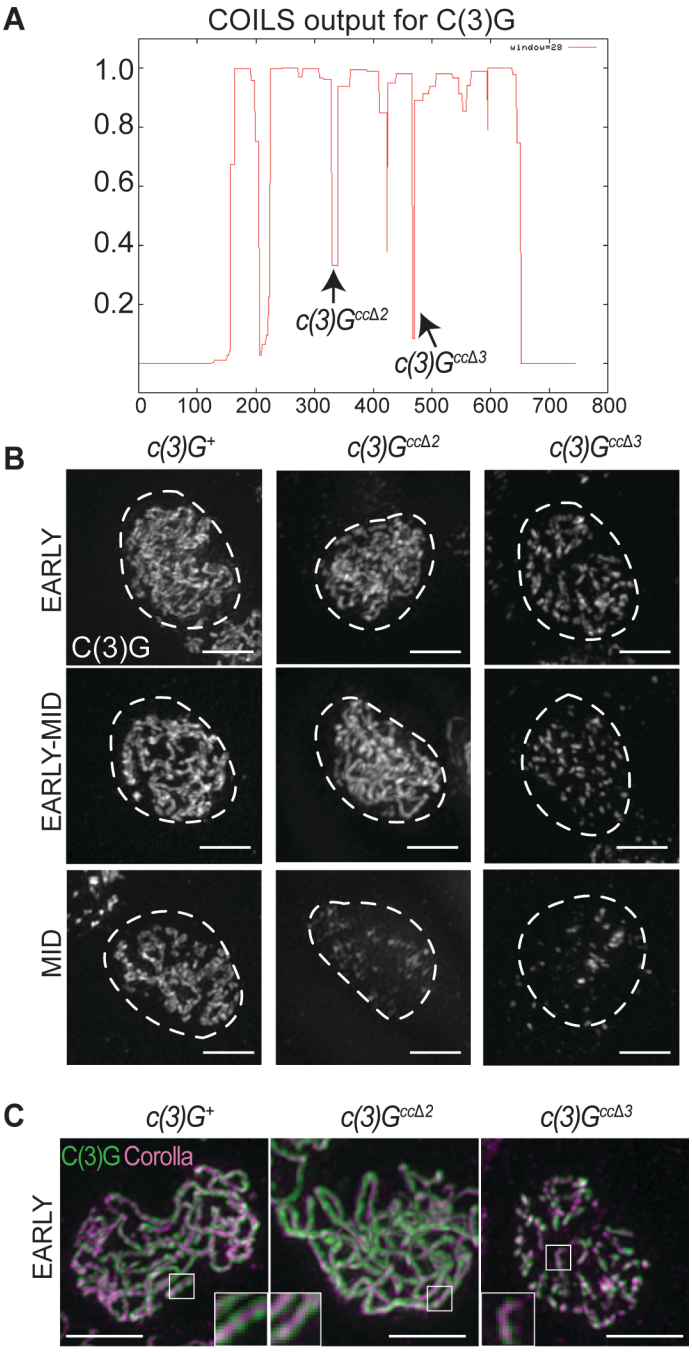

Figure 4- figure supplement 1: C(3)G is present in *c(3)G^{ccΔ2}* and *c(3)G^{ccΔ3}* mutants.

(A) Diagram of COILS score along the length of C(3)G with arrows where *c(3)G^{ccΔ2}* and *c(3)G^{ccΔ3}* deletions were made (Lupas et al., 1991). (B) Images showing localization of the SC protein C(3)G in wild type, *c(3)G^{ccΔ2}*, and *c(3)G^{ccΔ3}* flies from early pachytene (region 2A) to mid pachytene (region 3). Dotted lines indicate the location of the nucleus

as defined by DAPI staining (not shown). (C) Combined Corolla (magenta) and C(3)G (green) staining in early pachytene nuclei show localization of Corolla to the middle of C(3)G. Scale bars, 2 μm.

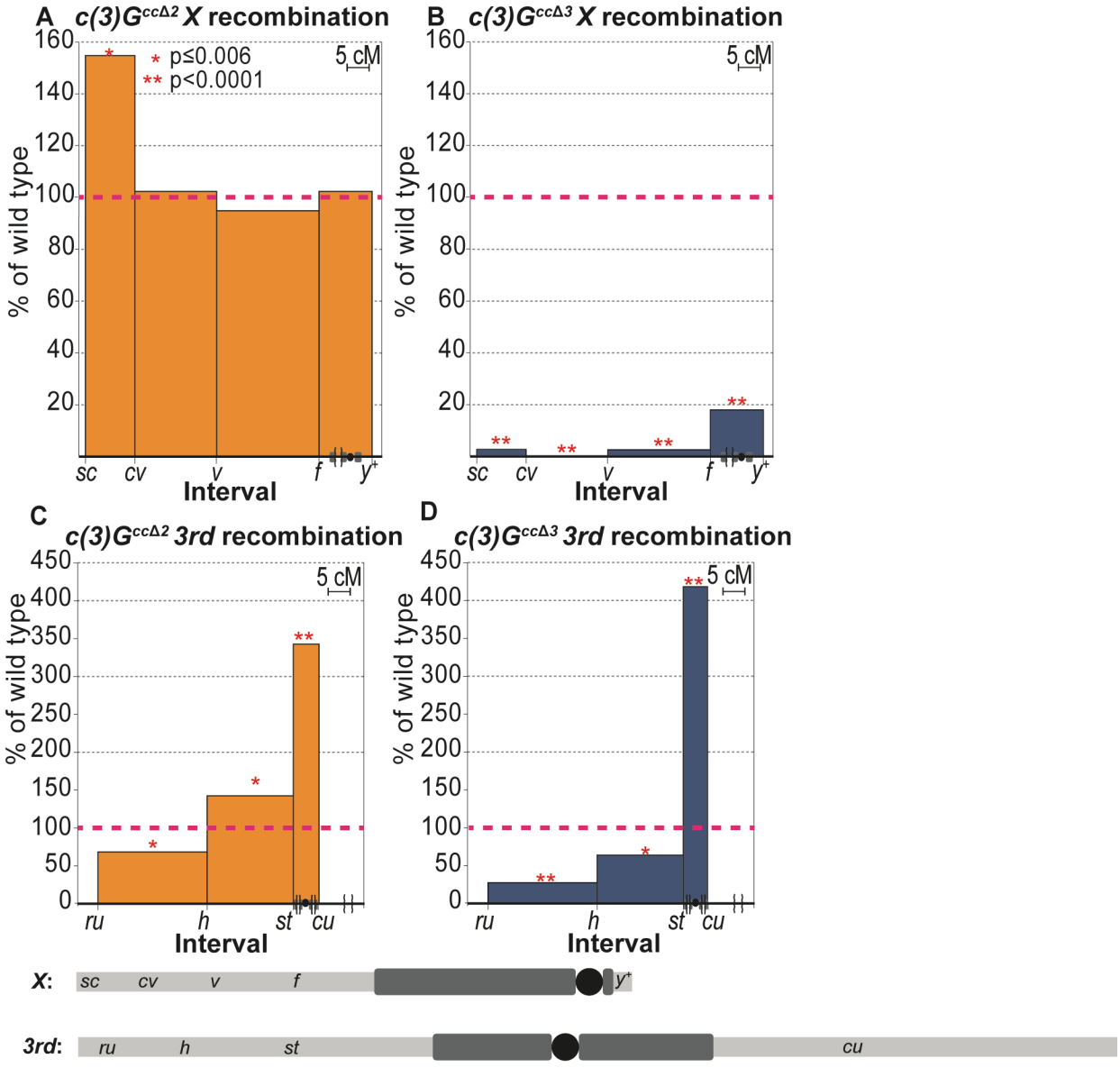

Figure 5: Loss of SC maintenance in *c(3)G*^{ccΔ2} mutants in mid pachytene is not sufficient to disrupt *X* chromosome recombination. Recombination in c*(3)G*^{ccΔ2} and c*(3)G*^{ccΔ3} females on the *X* chromosome (A,B) and the *3rd* chromosome (C,D) are plotted with percent of wild type on the y-axis vs chromosome location (in cM) on the x-axis. Brackets along x-axis indicate truncation of that region of the chromosome. The red dotted line marks wild type levels of recombination and is set at 100%. P-values

obtained using a Fisher's exact test (see Table 1,2 for N values). See Methods for the recessive markers used to assay recombination. For reference, below each chart is a diagram of the corresponding chromosome being analyzed displaying the relative cytological positions of the recombination markers and the approximate amounts of pericentromeric heterochromatin estimated from (Ashburner et al., 2005) (the black circle represents the centromere).

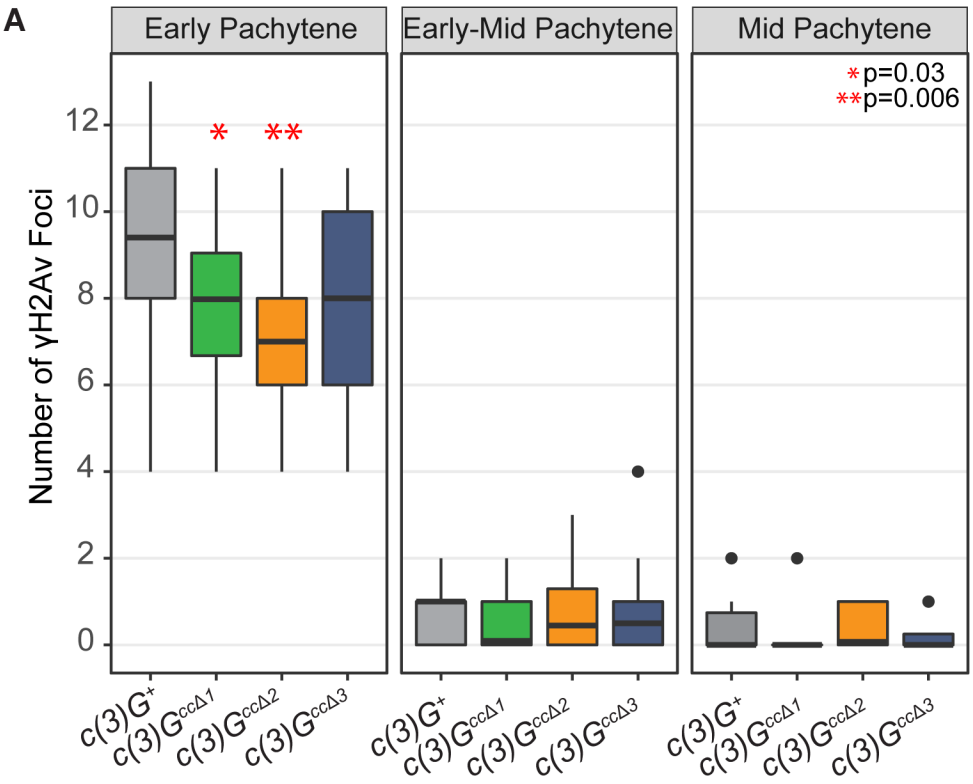

B

3rd chromosome recombination frequency

Genotype	*ru-h*	*h-st*	*st-cu*	total	N
c(3)G^{+}	23.0	21.7	6.1	50.9	525
c(3)G^{ccΔ3}	6.3	11.7	27.5	45.5	615
vilya^{826}*; +; c(3)G*^{ccΔ3}	0.5	0.0	0.9	1.4	214

Figure 5- figure supplement 1: DSB levels, as determined by γH2AV foci number, in *c(3)G*^{ccΔ1}, *c(3)G*^{ccΔ2} and *c(3)G*^{ccΔ3} mutants are similar to wild type.

(A) Quantification of the number of DSBs per nucleus was determined by counting the number of γH2AV foci in early, early-mid and mid pachytene of the germarium for *c(3)G*$^{+}$, *c(3)G*^{ccΔ1}, *c(3)G*^{ccΔ2} and *c(3)G*^{ccΔ3} flies. N value is ≥ 10 nuclei. Statistics were performed using the Mann-Whitney test. (B) *3rd* chromosome recombination frequency in *c(3)G*$^{+}$, *c(3)G*^{ccΔ3} and, *vilya*^{826}*;c(3)G*^{ccΔ3} double mutants. Data for *c(3)G*^{ccΔ3} is the same as shown in Figure 5 and Table 2.

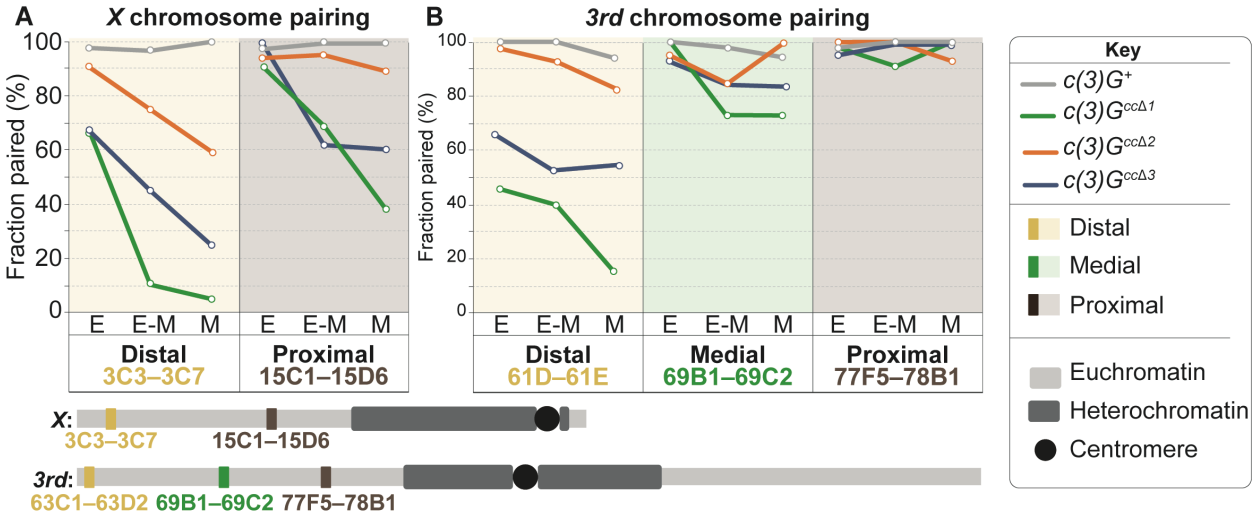

Figure 6: SC in early to mid pachytene maintains homologous chromosome pairing. Fraction of paired euchromatic regions in *c(3)G*$^{+}$ controls (grey line), *c(3)G*^{ccΔ1} (green line), *c(3)G*^{ccΔ2} (orange line), and *c(3)G*^{ccΔ3} flies (blue line) assessed by FISH using BAC probes against either centromere-distal or -proximal regions on the *X* chromosome (A) and centromere-distal, -medial or -proximal regions on the *3rd* chromosome (B) at early (E), early-mid (E-M) or mid (M) pachytene. For reference, below each chart is a diagram of the corresponding chromosome being analyzed (the black circle represents the centromere). For N-values see Table 5.

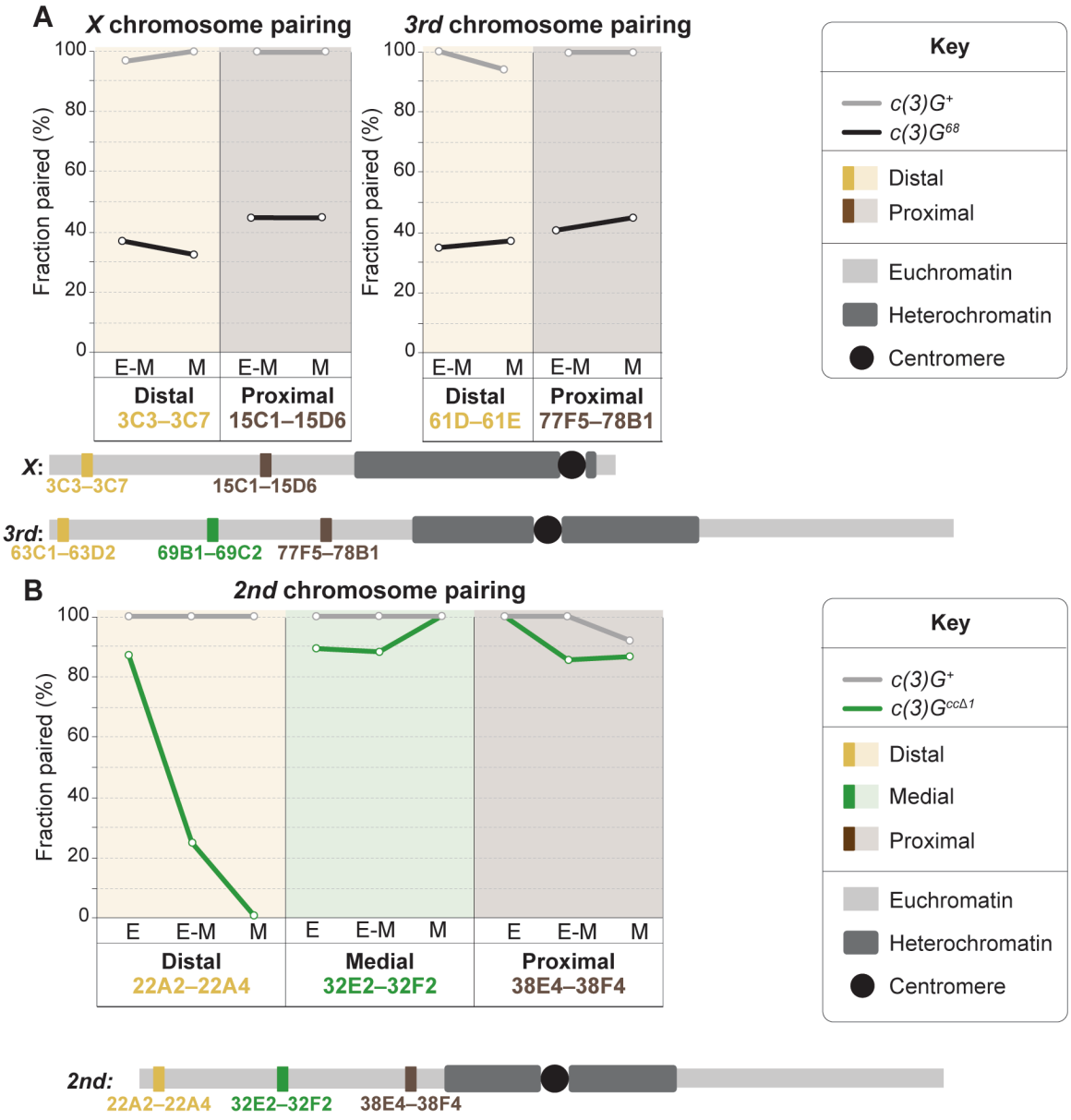

Figure 6- figure supplement 1: Pairing in *c(3)G*^{68} and *c(3)G*^{ccΔ1} mutants

(A) Fraction of paired euchromatic regions assessed by FISH using BAC probes against centromere-distal and proximal regions of the *X* and *3rd* chromosomes in *c(3)G*^{68} (black line) mutants at early-mid (E-M) or mid (M) pachytene. *c(3)G*$^{+}$ control data was previously presented in Figure 6. (B) Fraction of paired euchromatic regions on the *2nd*

1126 chromosome at early (E), early-mid (E-M) or mid (M) pachytene in *c(3)G*^{ccΔ1} (green line)

1127 mutants compared to *c(3)G*$^{+}$ (grey line) controls. See Table 5 for N values.

1128

1129

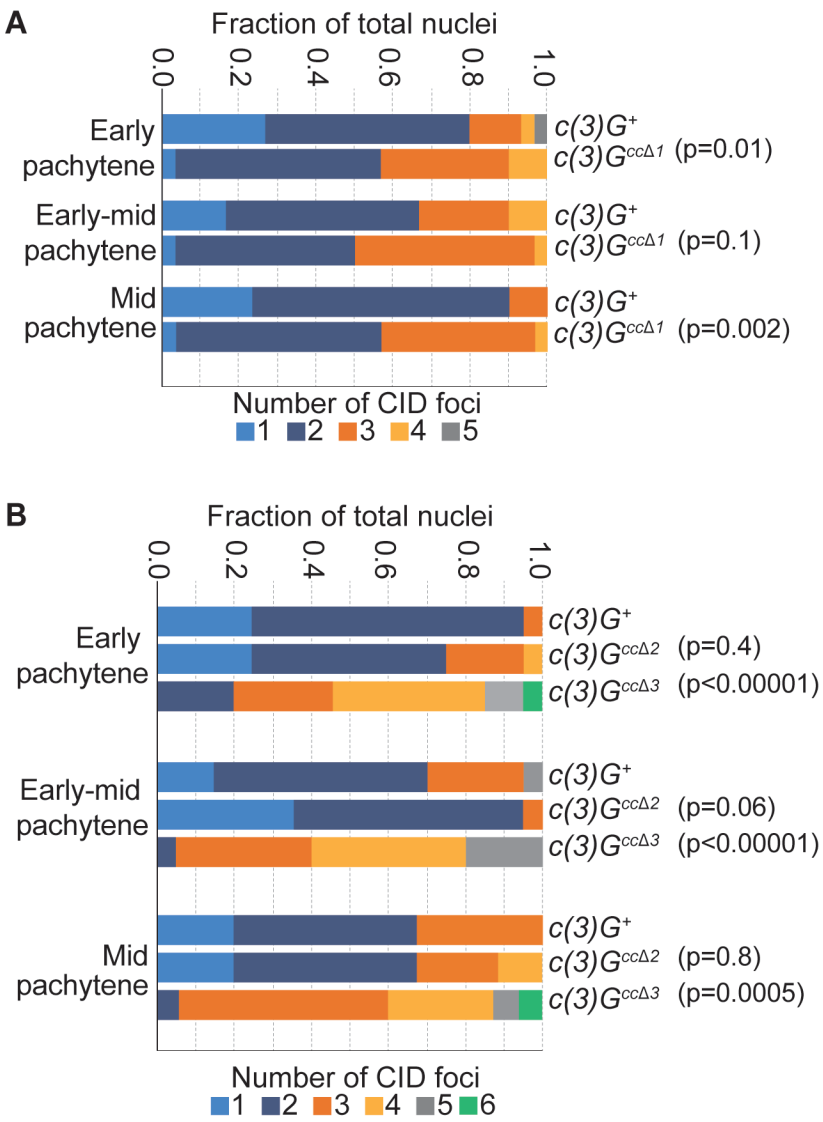

Figure 6- figure supplement 2: Centromere pairing *c(3)G*^{ccΔ1}, *c(3)G*^{ccΔ2}, and *c(3)G*^{ccΔ3} mutants

Quantification of the number of CID foci per nucleus in wild type, *c(3)G*^{ccΔ1}(A), *c(3)G*^{ccΔ2} (B), and *c(3)G*^{ccΔ3} mutants (B) from early pachytene (region 2A) to mid pachytene (region 3) shows no loss of centromere pairing. Statistics were performed using the Mann-Whitney test. N ≥ 15.

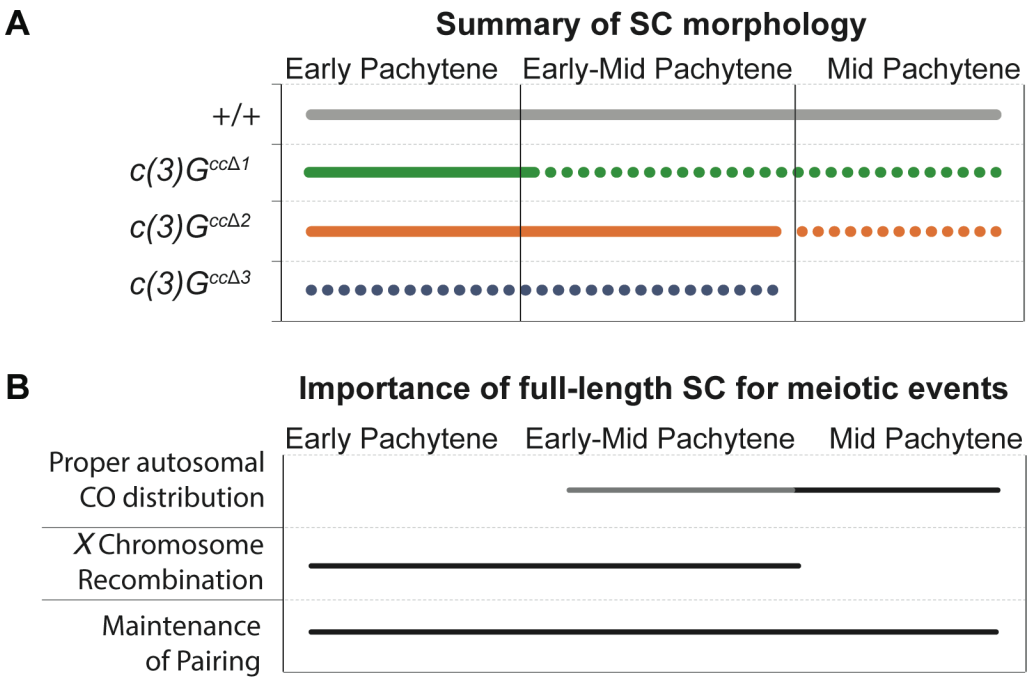

Figure 7: Summary of SC morphology and model of the requirement for SC in recombination and pairing maintenance.

(A) Summary of SC phenotypes in *c(3)G*$^{+}$ (grey line), *c(3)G*^{ccΔ1} (green line), *c(3)G*^{ccΔ2} (orange line) and *c(3)G*^{ccΔ3} (blue line) flies. *c(3)G*^{ccΔ1} flies displayed SC defects in early-mid pachytene while *c(3)G*^{ccΔ2} flies lost SC in mid pachytene. *c(3)G*^{ccΔ3} flies never fully assembled SC. Dotted line indicates defects in total SC length and fragmentation (B) A model of the requirement of full-length SC (black lines) at different stages of pachytene. Based on our data we propose that full-length SC is important for proper autosomal crossover placement, *X* chromosome recombination and maintenance of pairing at different stages of early to mid pachytene. The grey line represents a potential role for full-length SC that cannot be confirmed with our data.

Table 1. *X* Chromosome Recombination

Maternal genotype	$c(3)G^{+}$ (N=1515)	$c(3)G^{ccΔ1}$ (N=1420)	$c(3)G^{+}$ (N = 1721)	$c(3)G^{ccΔ2}$ (N = 1119)	$c(3)G^{ccΔ3}$ (N = 401)
Map Length (% compared to $c(3)G^{+}$)					
sc–cv	8.8	0.4 (4.5%)	10.6	16.6 (157%)	0.3 (2.8%)
cv–v	20.7	0.7 (3.4%)	18.1	18.5 (102%)	0.0 (0.0%)
v–f	21.1	5.2 (24.6%)	21.8	20.7 (95%)	0.5 (2.3%)
f–y^{+}	12.4	5.4 (43.5%)	11.2	11.5 (102%)	2.0 (17.9%)
Total	**63.0**	**11.8 (18.7%)**	**61.7**	**67.4 (109%)**	**2.8 (4.5%)**
Interference					
sc/cv/v	0.7	n/a*	0.5	0.8	n/a*
cv/v/f	0.6	n/a*	0.4	0.5	n/a*
Class					
NCO	688	1264	812	475	390
SCO	703	147	764	537	11
DCO	120	7	137	104	0
TCO	4	2	8	3	0
Exchange rank					
E_0	0.067	0.790	0.103	0.034	0.945
E_1	0.627	0.196	0.597	0.604	0.054
E_2	0.285	0.003	0.263	0.339	0
E_3	0.021	0.011	0.037	0.021	0

Abbreviations: N, total number of flies scored; NCO, chromatids recovered exhibiting no crossovers; SCO, single-crossover chromatids; DCO, double-crossover chromatids; TCO, triple-crossover chromatids. *Interference was not calculated unless there were at least 10 DCOs and was not calculated across the centromere. $c(3)G^{+}$ is *y w; pol.*

Table 2. 3rd Chromosome Recombination

Maternal genotype	*c(3)G*$^{+}$	*c(3)G*^{ccΔ1}	*c(3)G*$^{+}$	*c(3)G*^{ccΔ2}	*c(3)G*^{ccΔ3}
	(N=1014)	(N=1385)	(N = 1994)	(N = 931)	(N = 615)
Map Length (% compared to *c(3)G*$^{+}$)					
ru–h	22.5	13.1 (58.2%)	24.7	16.2 (65.5%)	6.3 (25.5%)
h–st	22.4	24.0 (107%)	18.9	26.6 (141%)	11.7 (61.9%)
st–cu	6.1	27.3 (447%)	6.8	23.6 (347%)	27.5 (404%)
Total	**50.9**	**64.4 (126%)**	**50.4**	**66.4 (141%)**	**45.5 (90.3%)**
Interference					
ru/h/st	0.7	0.5	0.8	0.6	n/a*
Class					
NCO	546	675	1069	418	377
SCO	421	535	842	411	199
DCO	45	167	83	99	36
TCO	2	8	0	3	3
Exchange rank					
E_0	0.165	0.202	0.155	0.111	0.343
E_1	0.665	0.420	0.678	0.477	0.442
E_2	0.154	0.345	0.166	0.387	0.176
E_3	0.016	0.032	0.000	0.026	0.039

Abbreviations: N, total number of flies scored; NCO, chromatids recovered exhibiting no crossovers; SCO, single-crossover chromatids; DCO, double-crossover chromatids; TCO, triple-crossover chromatids. *Interference was not calculated unless there were at least 10 DCOs in those intervals and was not calculated across the centromere. *c(3)G*$^{+}$ is *y w; pol.*

Table 3. 2^{nd} Chromosome Recombination

Maternal genotype	$c(3)G^{+}$ (N = 2376)	$c(3)G^{ccΔ1}$ (N = 1456)	
Map Length (% compared to $c(3)G^{+}$)			
net–dpp	5.7	3.4	(59.6%)
dpp–dpy	8.0	5.8	(72.5%)
dpy–b	28.5	26.9	(94.4%)
b–pr	7.8	24.9	(319%)
pr–cn	2.2	6.7	(304%)
Total	**52.2**	**67.6**	**(129%)**
net/dpp/dpy	0.3	0.8	
dpp/dpy/b	0.6	0.8	
dpy/b/pr	0.6	-0.2	
NCO	1249	624	
SCO	1021	692	
DCO	98	128	
TCO	8	12	
E_0	0.134	0.033	
E_1	0.715	0.648	
E_2	0.125	0.253	
E_3	0.027	0.066	

Abbreviations: N, total number of flies scored; NCO, chromatids recovered exhibiting no crossovers; SCO, single-crossover chromatids; DCO, double-crossover chromatids; TCO, triple-crossover chromatids. *Interference was not calculated unless there were at least 10 DCOs and was not calculated across the centromere. $c(3)G^{+}$ is *y w; pol.*

Table 4. *X* and *4th* Chromosome Nondisjunction

Maternal genotype	*c(3)G*$^{+}$	*c(3)G*^{ccΔ1}	*c(3)G*$^{+}$	*c(3)G*^{ccΔ2}	*c(3)G*^{ccΔ3}
	(N=1348)	(N=954)	(N = 1157)	(N = 2422)	(N = 837)
Percent nondisjunction (p value)					
X	0.7	1.5	1.0	0.5	4.5*
4th	0.4	0.6	0.1	0.1	2.0*

Rate of *X* and *4th* nondisjunction in *c(3)G*$^{+}$, *c(3)G*^{ccΔ1}, *c(3)G*^{ccΔ2}, and *c(3)G*^{ccΔ3} females. Significance calculated as described in (Zeng et al., 2010). Adjusted n accounts for the inviable progeny class plus the scored progeny. **c(3)G*^{ccΔ3} females display elevated rates of both *X* ($p < .001$) and *4th* ($p<.001$) nondisjunction when compared to *c(3)G*$^{+}$ controls; however the number of flies scored is not sufficient to determine significance.

Table 5. Summary of *X* and *3rd* chromosome pairing

Maternal genotype	*c(3)G*$^{+}$	*c(3)G*^{ccΔ1}	*c(3)G*^{ccΔ2}	*c(3)G*^{ccΔ3}	*c(3)G*^{68}
Percent paired (N value)					
X proximal (3C3-3C7)					
Early	97.1(70)	67.9(28)	90.9(33)	68.8(16)	n/a
Early-mid	96.6(60)	10.7(28)	75(20)	45(20)	37(27)
Mid	100(24)	5.3(19)	58.8(17)	26.3(19)	36.8(19)
X distal (15C1-15D6)					
Early	97.4(79)	90.6(32)	93.9(33)	100(17)	n/a
Early-mid	100(69)	69(29)	95(20)	62.5(16)	50(18)
Mid	100(28)	38.5(13)	88.2(17)	60(15)	53(15)
2nd proximal (22A2-22A4)					
Early	100(21)	87.5(24)	n/a	n/a	n/a
Early-mid	100(20)	25(20)	n/a	n/a	n/a
Mid	100(13)	1(9)	n/a	n/a	n/a
2nd medial (32E2-32F2)					
Early	100(21)	89.7(29)	n/a	n/a	n/a
Early-mid	100(15)	88.2(17)	n/a	n/a	n/a
Mid	100(8)	100(7)	n/a	n/a	n/a
2nd distal (38E4-38F4)					
Early	100(25)	100(37)	n/a	n/a	n/a
Early-mid	100(23)	85.7(28)	n/a	n/a	n/a
Mid	92.3(13)	86.7(15)	n/a	n/a	n/a
3rd proximal (61D-61E)					
Early	100(36)	45.8(24)	97.6(41)	68.4(19)	n/a
Early-mid	100(32)	40(20)	92.9(28)	52.6(19)	29.2(24)
Mid	93.8(16)	15.4(13)	83.3(24)	56.3(16)	40(15)
3rd medial (69B1-69C2)					
Early	100(46)	100(33)	95.5(22)	93.3(30)	n/a
Early-mid	97.6(43)	73.1(26)	85.7(14)	86.7(15)	n/a
Mid	94.4(18)	73.6(19)	100(9)	84(25)	n/a
3rd distal (77F5-78B1)					
Early	98.2(56)	98.1(54)	100(21)	96(25)	n/a
Early-mid	100(50)	90.9(33)	100(15)	100(17)	41.6(24)
Mid	100(20)	100(17)	93.8(16)	100(18)	50(16)

1233 **Key Resource Table**

RESOURCE/ REAGENT	SOURCE	IDENTIFIER
Antibodies		
C(3)G mouse C-terminal monoclonals	Hawley Lab	1A8-1G2 5G4-1F1 1G5-2F7
Corolla rabbit	Hawley Lab	AP-Corolla
CID rat	Gift from Claudio Sunkel	
CID rat	Hawley Lab	
γH2AV mouse	Iowa Hybridoma Bank	UNC93-5.2.1
Alexa Fluor 488 goat anti-mouse	ThermoFisher	A11001
Alexa Fluor 555 goat anti-mouse	ThermoFisher	A21422
Alexa Fluor 647 goat anti-mouse	ThermoFisher	A21235
Alexa Fluor 488 goat anti-rabbit	ThermoFisher	A11008
Alexa Fluor 555 goat anti-rabbit	ThermoFisher	A21428
Alexa Fluor 555 goat anti-rat	ThermoFisher	A21434
Alexa Fluor 647 goat anti-rat	ThermoFisher	A21247
Bacterial Strains		
TOP10 chemically competent cells	ThermoFisher	C404003
Drosophila BAC RP98-28O9 (polytene band 22A2-22A4)	Children's Hospital Oakland Research Institute (CHORI)	RP98-28O9
Drosophila BAC RP98-43K24 (polytene band 32E2-32F2)	CHORI	RP98-43K24
Drosophila BAC RP98-7D17 (polytene band 38E4-38F4)	CHORI	RP98-7D17
Drosophila BAC RP98-2N23 (polytene band 61D-61E)	CHORI	RP98-2N23
Drosophila BAC RP98-26C20 (polytene band 69B1-69C2)	CHORI	RP98-26C20
Drosophila BAC RP98-3J2 (polytene band 77F5-78B1)	CHORI	RP98-3J2
Drosophila BAC RP98-3D13 (polytene band 3C3-3C7)	CHORI	RP98-3D13
Drosophila BAC RP98-9H1 (polytene band 15C1-15D6)	CHORI	RP98-9H1
Chemicals and Reagents		
AarI restriction enzyme	ThermoFisher	ER1581
SapI restriction enzyme (also known as LguI)	ThermoFisher	ER1931
Antarctic phosphatase	New England Biolabs	M0289S
T4 DNA ligase	New England Biolabs	M0202S
BbsI restriction enzyme	New England Biolabs	R0539S

AluI restriction enzyme	New England Biolabs	R0137S
HaeII restriction enzyme	New England Biolabs	R0107S
MseI restriction enzyme	New England Biolabs	R0525S
RsaI restriction enzyme	New England Biolabs	R0167S
SpeI restriction enzyme	New England Biolabs	R0133S
NdeI restriction enzyme	New England Biolabs	R0111S
MboI restriction enzyme	New England Biolabs	R0147S
MspI restriction enzyme	New England Biolabs	R0106S
Nonidet-P40	Sigma-Aldrich	11332473001
16% Formaldehyde	Electron Microscopy Sciences	15710
Prolong Gold	Life Technologies	P36930
2,2-thiodiethanol (TDE)	VWR	700008-210
VECTASHIELD	VWR	101098-042
Glycogen	ThermoFisher	10814010
Critical Commercial Assays		
Quik Change II XL Site-Directed Mutagenesis Kit	Stratagene/Agilent Technologies	200521
Zero Blunt TOPO Kit	ThermoFisher	451245
NEBuilder HiFi DNA Kit	New England Biolabs	E5520S
Illustra GenomiPhi V2 DNA Amplication Kit	GE Healthcare	GE 25-660-30
ULYSIS AF647 Nucleic Acid Labeling Kit	ThermoFisher	U21660
ULYSIS AF546 Nucleic Acid Labeling Kit	ThermoFisher	U21652
Centri-Sep Columns	Princeton Separation	CS-900
Qubit dsDNA HS assay kit	ThermoFisher	Q32851
QIAGEN Plasmid Midi Kit	QIAGEN	12143
Deposited Data		
Stowers Original Data Repository (ODR)	Stowers Institute for Medical Research	http://www.stowers.org/research/publications/odr
Stowers ImageJ Custom Plugins	Stowers Institute for Medical Research	research.stowers.org/imagejplugins/zipped_plugins.html
Experimental Model: Drosophila stocks used		
y w; +/+; +/+; sv$^{spa\text{-}pol}$	Hawley Lab	Wild Type (WT)
y w/Y^{+y}; Sp/SM1; sv$^{spa\text{-}pol}$	Hawley Lab	
FM7w; sv$^{spa\text{-}pol}$	Hawley Lab	
y w/Y^{+y}; Pr/TM3; sv$^{spa\text{-}pol}$	Hawley Lab	
FM7w/sc cv v f y^{+}; D/TM3	Hawley Lab	
y m{VASA-Cas9-3xGFP}ZH-2A-3xRFP w^{1118}/FM7c	Bloomington Stock Center	BLM 51323
y w; nosCas9	Bestgene	
y w; c(3)G ^{ccΔ1}ca/TM3; sv$^{spa\text{-}pol}$	Hawley Lab	

y w/w^{+}; ru h th st cu c(3)G^{ccΔ1}ca/TM3; sv$^{spa-pol}$/+	Hawley Lab	
yw; ru h th st cu c(3)G ^{ccΔ1}/TM3; pol	Hawley Lab	
yw; +/CyO; ru h th st cu c(3)G ^{ccΔ1}ca/TM3	Hawley Lab	
y w; c(3)G ^{ccΔ2}ca/TM3; sv$^{spa-pol}$		
yw; ru h th st cu c(3)G ^{ccΔ2}/TM3; pol		
y w; c(3)G ^{ccΔ3}ca/TM3; sv$^{spa-pol}$		
yw; ru h th st cu c(3)G ^{ccΔ3}/TM3; pol		
net dpp dpy b pr cn	Hawley Lab	
ru h th st cu sr e ca	Hawley Lab	KAC81
attached-XY, y^{+} v f B; C(4)RM, ci ey^{R}	Hawley Lab	AD1
sc cv v f y^{+}/Bar[S]Y	Hawley Lab	U106
w^{1118}; In(2LR)Gla, wg^{Gla-1}/CyO; Herm{3xP3-ECFP,αtub-piggyBacK10}M10	BLM 32073	Transposase
Oligonucleotides		
tataCACCTGCattaCCGAcgctagtggctcctaga gttcag	Ordered from IDT	Forward primer to PCR AarI C(3)G fragment *c(3)G ^{ccΔ1}* (ckc102)
gcagCACCTGCgcggTTAAtgaaaaagaatttata agtcttaccattaggttatc	Ordered from IDT	Reverse primer to PCR AarI C(3)G fragment *c(3)G ^{ccΔ1}* (ckc103)
gccgGCTCTTCNTAAccttttttctacaaaatgatttatt	Ordered from IDT	Forward primer to PCR SapI C(3)G fragment *c(3)G ^{ccΔ1}* (ckc104)
gtatGCTCTTCNCGGtcatcaaaacatagtttagtat cg	Ordered from IDT	Reverse primer to PCR SapI C(3)G fragment *c(3)G ^{ccΔ1}* (ckc105)
CTTCGAAAGCTTTGTTGGCCTCTAT	Ordered from IDT	Sense primer for gRNA plasmid *c(3)G ^{ccΔ1}* (ckc113)
AAACATAGAGGCCAACAAAGCTTTC	Ordered from IDT	Antisense primer for gRNA plasmid *c(3)G ^{ccΔ1}* (ckc114)
CTTCGCTCAATGCGATCTTCAAGCTGG	Ordered from IDT	Sense primer for gRNA plasmid *c(3)G ^{ccΔ2}*
AAACCCAGCTTGAAGATCGCATTGAGC	Ordered from IDT	Anti-sense primer for gRNA plasmid *c(3)G ^{ccΔ2}*
CTTCGATTGACTGATCAGGCAACGAGG	Ordered from IDT	Sense primer for gRNA plasmid *c(3)G ^{ccΔ2}*

AAACCCTCGTTGCCTGATCAGTCAATC	Ordered from IDT	Anti-sense primer for gRNA plasmid *c(3)G* ^{ccΔ2}
CTTCGCTCTTCCTGATTGCTGCGATGG	Ordered from IDT	Sense primer for gRNA plasmid *c(3)G* ^{ccΔ3}
AAACTCGCAGCAATCAGGAAGAGC	Ordered from IDT	Anti-sense primer for gRNA plasmid *c(3)G* ^{ccΔ3}
CTTCTCTTGAACAACAATCTGTCAAGG	Ordered from IDT	Sense primer for gRNA plasmid *c(3)G* ^{ccΔ3}
AAACTGACAGATTGTTGTTCAAGAC	Ordered from IDT	Anti-sense primer for gRNA plasmid *c(3)G* ^{ccΔ3}
gggttacactggctttcctt	Ordered from IDT	Genotyping primer for *c(3)G* ^{ccΔ3}
ctgagactgtaattcctcgctaaa	Ordered from IDT	Genotyping primer for *c(3)G* ^{ccΔ3}
accaacctcgtaggcatctg	Ordered from IDT	Genotyping primer for *c(3)G* ^{ccΔ2}
GTTGAGAAGAAAAATTCAGAGCTCCG	Ordered from IDT	Genotyping primer for *c(3)G* ^{ccΔ2}
Recombinant DNA		
pU6-BbsI-chiRNA-X204upstream	Vector backbone from Addgene	ID:45946
pHD-pBac-DsRed-X204HR	Vector backbone was a gift from Kate O'Conner-Giles Lab	
Software and Algorithms		
ImageJ	https://imagej.nih.gov/ij/	
Custom ImageJ plugins	research.stowers.org/imagejplugins/zipped_plugins.html	

1234